Michigan Technological University

Digital Commons @ Michigan Tech

Dissertations, Master's Theses and Master's Reports

2018

ELECTRO-MECHANICAL-THERMAL MODELING AND STABILITY OF PULSED POWER LOADS ON A DC NETWORK

Joshua Allen Dillon
Michigan Technological University, jadillon@mtu.edu

Copyright 2018 Joshua Allen Dillon

Recommended Citation

Dillon, Joshua Allen, "ELECTRO-MECHANICAL-THERMAL MODELING AND STABILITY OF PULSED POWER LOADS ON A DC NETWORK", Open Access Master's Thesis, Michigan Technological University, 2018.
https://digitalcommons.mtu.edu/etdr/573

Follow this and additional works at: https://digitalcommons.mtu.edu/etdr

 Part of the Controls and Control Theory Commons, and the Power and Energy Commons

ELECTRO-MECHANICAL-THERMAL MODELING AND STABILITY OF PULSED POWER LOADS ON A DC NETWORK

By

Joshua A. Dillon

A THESIS

Submitted in partial fulfillment of the requirements for the degree of

MASTER OF SCIENCE

In Electrical Engineering

MICHIGAN TECHNOLOGICAL UNIVERSITY

2018

© 2018 Joshua A. Dillon

This thesis has been approved in partial fulfillment of the requirements for the Degree of MASTER OF SCIENCE in Electrical Engineering.

Department of Electrical and Computer Engineering

Thesis Advisor:	*Dr. Wayne Weaver*
Committee Member:	*Dr. Lucia Gauchia*
Committee Member:	*Dr. John Pakkala*
Committee Member:	*Dr. Gordon Parker*
Department Chair:	*Dr. Daniel Fuhrmann*

Table of Contents

List of figures

List of tables

Acknowledgements

I would like to thank my adviser, Dr. Wayne Weaver, for his guidance through the course of my master's degree.

Additionally, I would like to thank the Air Force Research Laboratory for the opportunity to work on a portion of their projects.

Lastly, I would like to thank my parents Greg and Barb for their continued support throughout my undergraduate and graduate career at Michigan Technological University.

Definitions

Electrical Constants and Variables

λ_s – Source Boost Converter Duty Cycle Control (Time Average)
λ_m – Motor Buck Converter Duty Cycle Control (Time Average)
L_s – Source Boost Converter Inductor
L_m – Motor Buck Converter Inductor
R_{Lso} – Source Boost Converter Inductor Series Resistance
R_{Lm} – Motor Buck Converter Inductor Series Resistance
R_{Cbo} – Constant Load
C_b – Source Boost Converter Capacitor
u_s – Voltage Energy Storage Device
u_b – Current Energy Storage Device
v_s – Voltage Source
$i_{Ls}(t)$ – Source Boost Converter Current (Time Varying)
$i_{Lm}(t)$ – Motor Buck Converter Current (Time Varying)
$v_{Cb}(t)$ – Aircraft Bus Voltage (Time Varying)
$P_{load}(t)$ – Pulsing Power Load (Time Varying)

Mechanical Constants and Variables

k_m – Motor Current Torque Constant
J_m – Motor Mass Moment of Inertia
D_m – Motor Damping Coefficient
γ_m – Pump Load Coefficient
$\omega_m(t)$ – Motor Pump Rotational Speed (Time Varying)

Thermal Constants and Variables

m_{RLs} – Thermal Constant
T_0 – Initial Temperature
T_{sw} – Thermal Storage Temperature
R_{12} – Thermal Constant
R_u – Thermal Constant
$C_{\theta 1}$ – Weapon Mass Thermal Capacitance
$C_{\theta 2}$ – Return Fluid Mass Thermal Capacitance
α_m – Pump Mass Volume Coefficient
k_{rg} – Pulse Load Thermal Gain
$T_C(t)$ – Weapon Mass Temperature (Time Varying)
$T_R(t)$ – Return Fluid Temperature (Time Varying)

Pulsing Load

T_P – Pulse Period
A_P – Pulse Amplitude
D_P – Pulse Duty Cycle

List of abbreviations

EMT – Electro-Mechanical-Thermal

DEW – Direct Energy Weapon

PWM – Pulse Width Modulation

CPL – Constant Power Load

MEA – More Electric Aircraft

ESR – Equivalent Series Resistance

PPE – Peak Pulse Energy

EPHF – Equivalent Power Higher Frequency

HPHF – Higher Power Higher Frequency

Abstract

Modern military aircraft are developing larger pulsed power loads varying from new weapon technologies to advanced avionics and other electrical equipment. Pulsing power loads emulate a pulse width modulated signal which have non-linear destabilizing effects on the electrical system. Additionally, these devices have thermal properties that can induce electrical stability issues at low and high temperatures and various pulsing load conditions. These non-linear electrical stability issues carry through to the mechanical and thermal systems of the aircraft and can damage components. The MATLAB/Simulink workspace is used to simulate a non-linear model of an aircraft's electrical-mechanical-thermal (EMT) system. This system includes electrical generation with constant and pulsing power loads, mechanical fluid pumping, and thermal cooling systems.

The goal of the EMT model is to demonstrate the destabilizing effects caused by both the thermal coupling of the pulsing load and the large signal analysis of the PWM signal. An operational boundary of the power pulsed device is found by varying the duty cycle for a given pulse period and power load based on bus voltage transients and voltage drop limits. The system is defined metastable for a given set of parameters if the system experiences periods of stability and instability based on varying operating points. Regions of complete stability, metastability, marginal metastability, and instability are determined based on bus voltage transient tolerances. Analyzing the marginally metastable boundary layer, thermal analysis is performed at different points of equivalent average power and varying pulse energy. Post processing the results determines the most efficient operational region of the system given thermal and electrical requirements.

1 Background

The More Electric Aircraft (MEA) program is continuously evolving, and over the past several years new military aircraft are developing orders of magnitude greater power demands as compared to aircraft from a decade ago. Simulation tools have been used to categorize aircraft electrical systems and electrical system requirements with a focus towards pulsing power devices. These pulse power devices can be laser weapons, electromagnetic devices, or other high energy devices that induce a large load on the aircrafts electrical bus [1, 2]. With new electrical power demands come new thermal management demands that require consideration during the design phase of the system. These new technologies can have large heat dissipation requirements requiring more than 1MW of heat power management and various forms of thermal management strategies [3] [4].

Aircraft developed through the MEA program are aircraft where secondary loads that are traditionally powered via secondary mechanical energy sources are moved to a controlled electrical source. It is presented in [5] the types of loads that are demanded from an electrical system onboard a MEA. These include hydraulic systems and engine accessories such as fuel pumps. This adds complexity and demand on the electrical system of the aircraft, requiring new power management and distribution topologies. The more recent electrical systems typically consist of generation source, DC-DC boost converter, and some sort of energy storage device as seen in [6]. Some additional reasons for converging towards MEA topology, both in civilian and military aircraft, are shared with hybrid and battery electric vehicles [7]. Striving towards electrically controlled devices

allows for a more precise control of systems allowing the vehicle to have better fuel efficiency. This specifically benefits military aircraft by allowing the aircraft to have better combat effectiveness and increased range.

Devices such as a Direct Energy Weapon (DEW), which are time varying pulse power loads, are best defined as a pulse width modulated (PWM) signal with a varying period, duty cycle, and magnitude. [8] demonstrates that PWM signals induce unpredictable stability issues in closed loop systems. Other analysis techniques replace the PWM source with an energy equivalent constant power load (CPL), performing small signal analysis (linear or continuous signal-based analysis). Small signal analysis allows for linear analysis techniques to be used rather than understanding the complete dynamics of the non-continuous PWM load. Some research has taken place with respect to defining the stability boundary of a system given a CPL [9]. These results show the stability of the aircraft bus voltage with constant power values that step up and down in magnitude. These results capture the steady state dynamics of the step input but not the pulsing of the power load.

A time varying pulse power load with large signal (non-continuous) analysis on a system yields more accurate results than those of small signal analysis. These types of experiments help in understanding of the dynamics of a non-linear system [10]. Research has been carried out on the pulse load application with respect to naval applications and the more electric ship initiative (MES) [11]. Large naval ships have advanced electromagnetic magnetic rail systems (EMALS) to launch aircraft instead of the conventional steam catapult systems. The operational boundary of the device is determined by determining instability boundaries and operational limits given a pulse width, period, and duty cycle. These new naval warfare ships also have other electromagnetic weapon

systems that are pulse power devices which undergo large signal analysis. These systems induce a large load on the ships electrical bus and cause stability issues in the bus voltage [12].

One process that has been used to analyze non-linear pulse power systems is called Hamiltonian Surface Shaping and Power Flow Control (HSSPFC). This is a two-step method used for developing a control design for non-linear systems, such as what's seen in [13, 14]. This is also explored in [12] with the pulsing load on the MES as caused by the large signal analysis of the EMALS. These examples employ Lyapunov based control strategies which require the creation of an energy like function. With the pulse power device analyzed in [12] the model characterized is strictly an electrical model focusing on the large signal analysis of the pulsing device.

It is well known that thermal properties can have feedback effects to the electrical system that must be accounted for during the design and analysis of an aircraft's electrical system. In [15] the military standard MIL-STD-2218 presents maximum operating temperature range for power electronic devices used to power pulse loads. It states that current IGBT transistors have a maximum operating temperature of 125°C where Silicon Carbide and other developing transistors are expected to have operating temperatures of 350°C. It also presents different forms of cooling strategies for the power electronic devices and equipment. These include forced air via fans or ram air intakes which are less desirable due to developing outside heat signatures. Other forms include closed loop cooling using polyalphaolefin (POA) and water. These are comparable to conventional cooling methods using liquid to air heat exchangers. These have additional disadvantages as the aircraft

would then be forced to carry weight that would take away from ordinance or fuel capacity and reduce fuel efficiency.

This thesis uses JP8, known as aviation fuel, as the coolant for the system using the fuel tank as a thermal storage device. This method presents several advantages including reduced complexity and elimination of an external heat signature. A similar approach to cooling the system is seen in [16] where fuel is pumped through the device in a closed loop system. Thermal analysis of JP8 has been performed to determine the maximum amount of heat that can be added to the fuel [17] . Aviation fuel is often used to cool other components onboard the aircraft for the same reasons as pulsed power devices. [17] gives upper temperature limits for JP8 and JP8 with fuel additives, 163°C and 218°C respectively.

Instances of thermally variable electrical systems include power electronic devices such as boost and buck converters, commonly seen on MEA. It's well documented that power electronic devices and MOSFETs have temperature requirements that cause efficiency and stability issues. [18] shows that the "on" resistance of a switching device is much less when the device is at a cooler operating temperature. This "on" resistance is the total resistance that is induced while current is flowing through the transistor. This resistance causes a voltage drop, power loss, and excess heat which then requires thermal management.

Other devices that are known to experience temperature coupled power issues are batteries and energy storage devices. These devices typically have low and high temperature requirements that affect their performance and longevity [19]. [20] explores modeling the thermal implications of power flow through the battery by assessing the

amount of heat energy dissipated. This presents that the current waveform performs as simulated, but the voltage waveform experiences a voltage drop while loaded. If the battery were to be connected to a grid or bus, additional thermal based control would need to be implemented.

Pulse power loads on an aircraft are powered by mechanical generation from a secondary power source and battery system. Some battery pulse power applications can be seen in the automotive field with new and developing electric vehicles [21]. Some batteries have had pulsed power loads tested on them at specific temperatures as in [22]. An important observation is the battery has an internal resistance that affects the voltage output from the cells to the terminals. This resistance is non-linear and a function of temperature, state of charge, and load on the battery. Systems such as these can are examples of perturbed non-linear systems. Perturbations are a focus of non-linear control strategies and are defined as a small change to the system that has a large implications on the output [23].

2 Introduction

There has been much research that has focused on the electrical stability analysis with pulsing electrical loads. These pulsing loads have been analyzed on an individual component level and the complete electrical system. Additional research has put forth into quantifying some of these results by use of HSSPFC to develop a comprehensive Lyapunov based control strategy. Thermal based electrical analysis has taken place on power electronic and storage devices with focus on heat management. There has been limited research put into understanding the dynamics of an interconnected electrical, mechanical, and thermal system. Traditionally analysis is on a single aspect of a complete system, such as studying the electrical dynamics or the thermal properties of a device. Studying a completely intertwined electric, mechanical, and thermal system offers new and unique perspectives.

This thesis provides the stability analysis of a pulsed power device with respect to the thermal characteristics and maximum energy output. The focus of analysis is on the time varying thermal coupling of the non-linear pulsed power device. This device resides onboard a MEA and is interconnected with the EMT system. The thermal coupling is analyzed as inducing series resistance to the supply current to the electrical system. The non-linear combination of a series thermal resistance and the large signal analysis of the pulsing load causes two focus points of stability analysis. Analyzing the maximum operating range of the device, it will be possible to determine the maximum pulse energy and average power output of the device. These operational boundaries will allow for additional analysis of the relationship between temperature and bus voltage transients.

A coupled electrical, mechanical, and thermal system has yet to be analyzed from the perspective of a pulsed power load and thermally coupled stability analysis. The emphasis on large signal analysis with thermal coupling from the pulsing load allows for a unique perspective of system analysis. This thermal coupling demonstrates the perturbation of the electrical system by thermal feedback of the pulsing weapon load. It is desired to define the operational stability boundary and determine the electrical and thermal limits of the DEW. It will define the boundary layer that separates the stable region of operation from the unstable region, metastable region, and marginally metastable boundary layer.

The perturbation of a system is a changing parameter where the magnitude of the change is small but has large implications. This is a focus of non-linear systems analysis that has its own strategies and techniques. These small changes to the system induce larger nontrivial dynamics that need to be analyzed to determine the total effects it causes on the system. MATLAB/Simulink is the simulation tool used to characterize the entire EMT system. This is done by developing a series of linear and non-linear non-autonomous state equations to capture the dynamics caused by the perturbations and large signal analysis of the load. It's predicted that the coupled EMT model will have stability issues at various temperatures and pulsed load throughout the region of operation.

3 System Model

The subsystem studied is an aircraft's electrical bus connected to mechanical pumps and thermal cooling loads with an emphasis on the large signal analysis of the pulsing load and thermal management system. The total electrical system consists of a supply voltage and generation source, DC-DC boost converter, constant power load, pulsing weapon power load, and a PMDC motor driven by a DC-DC buck converter. The PMDC machine drives the mechanical portion of the system, which is a cooling pump circulating coolant through the device and returning to a reservoir tank, creating a closed loop cooling system. A schematic of the model showing the electrical, mechanical, and thermal components is seen in Figure 1.

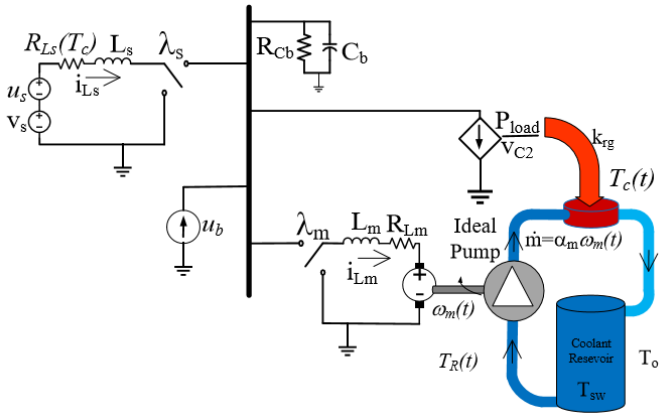

Figure 1. Schematic of electrical source, electrical and mechanical load, and heat power and cooling devices.

This DC micro-grid of the aircraft electrical bus is desired to be a nominal 270 V_{DC} from a source supply voltage of 135 V_{DC}. With this system studied, open loop control is

used for the boost converter duty cycle. Once dynamics and stability of the EMT are better understood, closed-loop control can be applied in future work. The nominal duty cycle of 50 % is used and remains unchanged for the duration of the experiments. The cooling pump PMDC machine is driven by a buck converter circuit which reduces the input bus voltage to desired output voltage. Throughout the experiments, the duty cycle for the buck converter is kept constant at 50 % resulting in a nominal supply voltage of 135 V_{DC}.

3.1 System State Equations

The model is mathematically defined by a series of three electrical, one mechanical, and two thermal states yielding 6 differential equations. The model of generation and current source DC-DC converter is written as

$$L_s i_{Ls}{}'(t) = -i_{Ls}(t)R_{Ls}(t) - \lambda_s v_{Cb}(t) + u_s + v_s \quad (1)$$

where there is non-linear coupling of current and time variant series resistance. The current differential is linked with the inductance of the inductor of the boost converter to yield the switched current to the bus. u_s is a current storage device that can supply or absorb current depending on the characteristics of the bus. Throughout the experiment its value is kept at a constant 0 A value. The nominal battery/generation voltage supply source is defined as v_s.

The series resistance that couples the temperature of the device to the electrical system, seen in (1), is defined as

$$R_{Ls}(T_C) = m_{RLs}(T_C(t) - T_0) + R_{Lso} \quad (2)$$

which doesn't explicitly add an additional state. This equation does incorporate the dynamics of the device temperature from (3). The coefficient of thermal coupling, m_{RLs},

relates the change in temperature to changes in resistance. The scaling of the difference between the device's initial temperature, T_0, and current value determines the resultant thermal resistance. This thermal resistance is summed with the inductor's equivalent series resistance (ESR) to yield the total series resistance. This ESR induces a voltage drop to the bus, increases resistive power losses, and causes thermally coupled electrical stability issues.

The thermal model of the system consists of one linear and one non-linear differential state equations based on the first law of thermodynamics. Defining the pulsing power device thermal equation as

$$C_{\theta 1} T_C{}'(t) = R_{12}(T_R(t) - T_C(t)) + k_{rg} P_{load}(t) \tag{3}$$

which linearly relates the device temperature (T_C) to the coolant temperature (T_R) and the magnitude of the load. The difference in temperature is scaled by the thermal R_{12} coefficient. This shows that if the fluid is cooler than the device it will act to cool the device and heat the device if the fluid is warmer. The power load thermal relation is achieved through a thermal coupling coefficient (k_{rg}) that translates electrical power to heat.

The non-linear coolant temperature state is defined as a measurement of the fluid after it has passed through to the device to absorb heat energy. This is mathematically written as

$$C_{\theta 2} T_R{}'(t) = R_{12}(T_c(t) - T_R(t)) + \alpha_m R_u \omega_m(t)\big(T_{sw} - T_R(t)\big). \tag{4}$$

Equation (4) links both the device temperature and fluid temperature in the same way as in (3). This equation also accounts for the difference in temperature between the fluid in the fuel tank and the returning fluid. The thermal storage tank temperature, T_{sw}, is held constant

as the volume of fuel being used as coolant is much less than the volume of fuel in the tank. The non-linearity exists in the link to the time varying motor speed ω_m, seen in equation (8). The mass flow rate of coolant is a function of the motor speed and the pumping coefficient α_m. The non-linearity exists in coupling the mass flow rate of coolant with the coolant return temperature. This mass flow rate is coupled via another coefficient, R_u, that relates the effectiveness of the heat transfer between the fluid and the tank temperature.

The bus voltage for the aircraft DC network is done by writing the KCL equation for the supply boost converter to the aircraft's electrical bus, seen as

$$C_b v_{Cb}'(t) = u_b - \frac{v_{Cb}(t)}{R_{Cbo}} - \frac{P_{load}(t)}{v_{Cb}(t)} - \lambda_m i_{Lm}(t) + \lambda_s i_{Ls}(t). \tag{5}$$

This relationship between a time varying bus voltage and pulsing load current is an instance of the large signal analysis of the pulsing load. This equation is non-linear due to the division of the bus voltage by the pulsing load, yielding a dynamic pulsed current. u_b is defined as a voltage energy storage device that can supply or absorb current depending the circuit requirements. Within this experiment, the value is kept at a constant 0 A but can be explored in future work. The fixed duty cycle for the buck converter supplying current to the motor, λ_m, is defined as a constant 50 % value. The duty cycle for the boost converter supplying current to the system, λ_s, is set at 50 %. If the duty cycle were changed, the control would be redefined as

$$\lambda_s = 1 - D_s \tag{6}$$

where D_s is the desired duty cycle.

A similar process is performed for writing the current going to the PMDC machine. KVL for the buck converter that controls the cooling pump is written as

$$L_m i_{Lm}'(t) = \lambda_m v_{Cb}(t) - R_{Lm} i_{Lm}(t) - k_m \omega_m(t). \quad (7)$$

The supply current to the motor (i_{Lm}) and pump can either be linearly related to the bus voltage of the system or cause additional non-linearity's depending on the control strategy of the converter. This relationship primarily shows that transients induced by the pulsing load will be translated to the supply current of the motor. This equation also accounts for the voltage drop caused by the ESR of the buck converter's inductor through R_{Lm}. The k_m constant converts the rotational speed of the motor to calculate the back electromagnetic field (EMF) voltage of the motor.

The non-linear differential state equation that defines the cooling pump speed of the system is written as

$$J_m \omega_m'(t) = -D_m \omega_m(t) + k_m i_{Lm}(t) - \gamma_m \omega_m(t)^2. \quad (8)$$

The pump speed (ω_m) is dependent on the current supplied to the motor and the load on the motor. This includes both the linearly dependent mass moment of inertia of the pump impeller and the non-linear load of viscous fluid being pumped. The current supplied from the bus drives the speed of the motor by way of the torque constant k_m. This model accounts for the damping (D_m) caused by the speed of the motor as well as the viscous fluid (coolant) load (γ_m).

3.2 Pulse Power Load

From (4), the current demanded by the load from the source is described by

$$i_p(t) = \frac{P_{load}(t)}{v_{Cb}(t)} \quad (9)$$

which interconnects the dynamics of the bus voltage and large signal interpretation of the load. This dynamic current will induce transients on the bus voltage and supply current when cycled and is one source of expected non-linearity. P_{load} is the magnitude of the pulse which cycles between the preset value and 0 W. i_p is the resultant time varying current signal demanded by the device. P_{load} is a non-continuous time variant function, which is inherently non-linear, and the division by the state of (5) results in (9) being a non-linear equation.

4 MATLAB/Simulink System Model

4.1 Simulation Construction

Developing the system of chapter 3 for analysis involved utilization of the MATLAB/Simulink workspace. The model and simulation created is divided into three connected parts. A MATLAB initialization file that contains variable declarations and logic for populating the surface plot variable. Creating a "master" MATLAB file in this way allows for flexibility to manipulate any part of the simulation at an efficient rate. The second portion is the Simulink model of the system pictured in Figure 1 and equations (1) through (9). Lastly, a MATLAB function was created to check for stability in the system. Each parameter in the definition chapter of this thesis have predetermined initial values and the time varying signals are given initial positive or zero values that represent the initial steady state. The constant and initial parameters of the electrical portion are in Table 1, mechanical portion in Table 2, and thermal portion in Table 3.

Each differential equation written is used to calculate the time varying values of current, voltage, speed, and temperature of the system. To properly evaluate these equations to determine the real time values, each differential equation is solved by use of integration. The non-autonomous non-linear system developed makes standard linear system analysis impossible as a state space model cannot be created. Writing the equations then required the use of a series of constant, sum, multiplication, and division blocks. Once the equations were assembled, a model solver type was chosen. The *"Ode4 (Runge-Kutta)"* fixed step solver was selected for all the experiments within this thesis.

Table 1. Electrical Parameter Values

Parameter	Value	Unit
λ_s	0.5	-
λ_m	0.5	-
L_s	3	mH
L_m	3	mH
R_{Lso}	0.025	Ω
R_{Lm}	0.025	Ω
R_{Cbo}	50	Ω
C_b	500	μF
u_s	0	Volts
u_b	0	Amps
v_s	135	Volts
$i_{Ls}(0)$	7.4	Amps
$i_{Lm}(0)$	3.02	Amps
$v_{Cb}(0)$	270	Volts
$P_{load}(0)$	0	Watts

Table 2. Mechanical Constants and Initial Values

Parameter	Value	Unit
k_m	3	N-m/Amp (V-s/rad)
J_m	0.01	kg·m^2
D_m	0.4	kg/s
γ_m	0.00015	kg
$\omega_m(0)$	22.5	rads/s

Table 3. Thermal Constants and Initial Values

Parameter	Value	Unit
m_{RLs}	0.006	Ω/°C
T_0	21	°C
T_{sw}	27	°C
R_{12}	25	-
R_u	10	Ω
$C_{\theta 1}$	1000	kg·m^2/K·s^2
$C_{\theta 2}$	100	kg·m^2/K·s^2
α_m	0.05	s/(rad-Ω)
k_{rg}	0.5	°C/W
$T_c(0)$	20	°C
$T_R(0)$	20	°C

4.2 Simulation Validation

To validate the model, open loop testing of the system is used as it's of interest to determine the areas of stability without added control. An initial load of 1000 W (P_{Load}), 1 s period (T_P), and 50 % duty cycle (D_P) are selected as a simple starting point. The simulated load power waveform can be seen in Figure 2**.** This load is used to analyze (1) through (9) focusing on the connected dynamics of the system and induced transients caused by the PWM load.

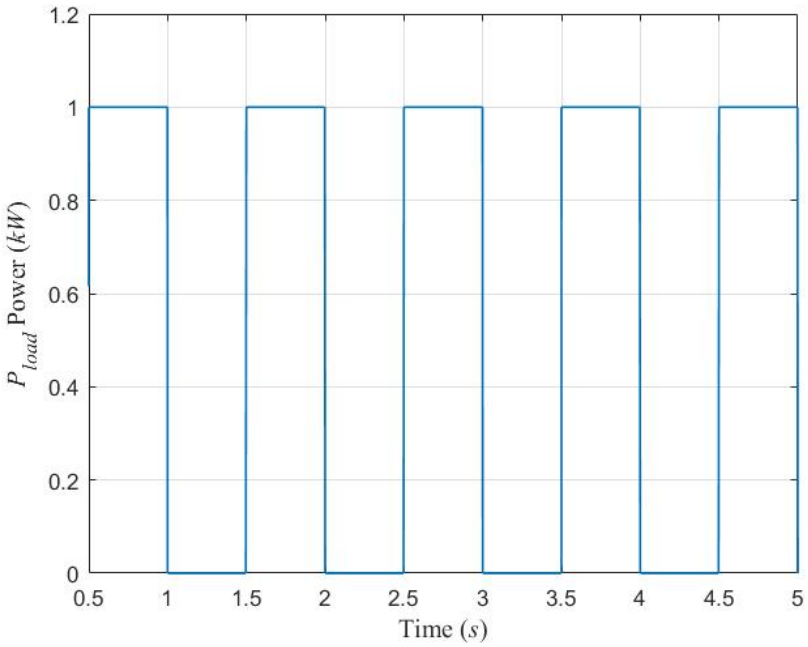

Figure 2. An initial load is set to test functionality of the Simulink model. The pulse load is set to 1000 W (P_{load}), 50 % duty cycle (D_P), and a pulse period (T_P) of 1 s.

The next equation analyzed in the simulation is the bus voltage of the system. Figure 3 shows the aircraft bus voltage over the same 4.5 s interval as Figure 2. It's noted that there are induced transients from the pulsed load that are damped out over the 500 ms interval before the load is cycled either on or off. The damping of these transients shows the stability of the bus voltage with the given load conditions. It's seen in this figure that the frequency of oscillation is 20 Hz. This is the natural, resonant, frequency of the complete EMT system. These oscillations are shown to affect every aspect of the subsystem.

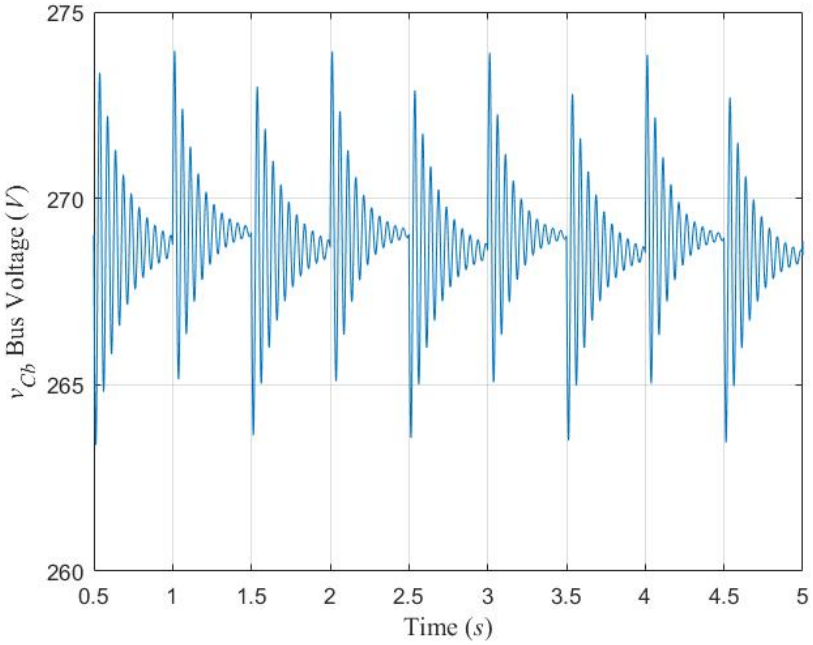

Figure 3. Resultant v_{Cb} bus voltage of the DC grid network on board the aircraft. Transients experienced damp out over time for both the pulsed load going high and low.

The simulated current supplied from the boost converter is seen in Figure 4. The current demanded pulses high and low with the pulsing load as expected. There is a nominal non-zero current during the pulse off period given the other constant loads on the bus. As with the bus voltage there are additional transients that occur when the load goes high and low that are damped out in the 500 ms intervals.

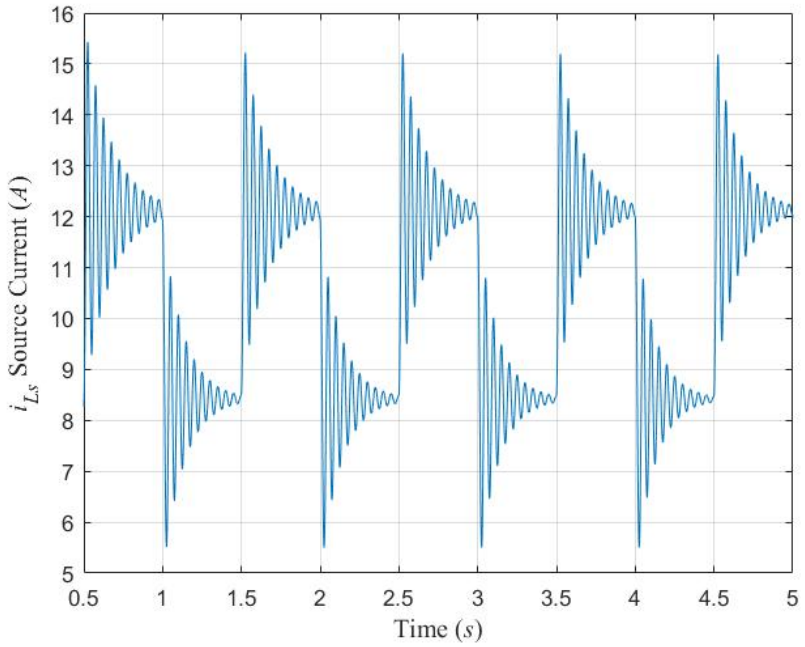

Figure 4. Resultant i_{Ls} source supply current of the DC grid network from the boost converter.

The cooling pump motor speed and supply current is seen in Figure 5. It's shown that even though the duty cycle control is fixed to the converter, the pump speed and motor current still deviate with the pulsed load. The bus voltage transients are translated to the supply current to the motor causing transients on the pump speed. This shows the large

signal analysis of the load induces periodic transients on the electrical and mechanical components of the aircraft system.

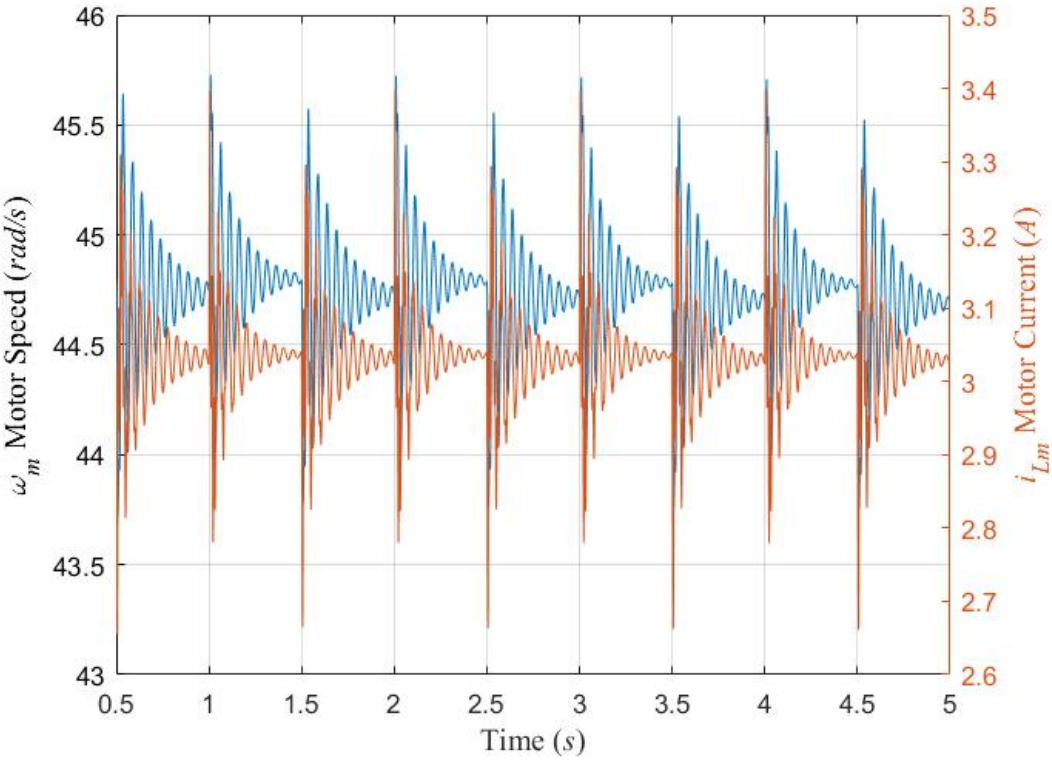

Figure 5. Cooling ω_m pump motor speed and i_{Lm} motor current showing the relationship between supply current and speed.

The temperature models for the pulse power device and return fluid can be seen in Figure 6 over the same 4.5 s interval. It's shown that when the pulsed load goes high the device temperature (T_C) increases. The cooling pump is acting to cool the device constantly as the motor is always pumping coolant. With only a low differential between the device and coolant temperature, a limited amount of cooling takes place. As the device temperature increases, the fluid temperature also increases following the dynamics of (3) and (4). During this initial startup region, the resultant waveforms appear to be linear.

When viewed over a longer timeframe an exponential curve is constructed. This is expected with a first order differential equation.

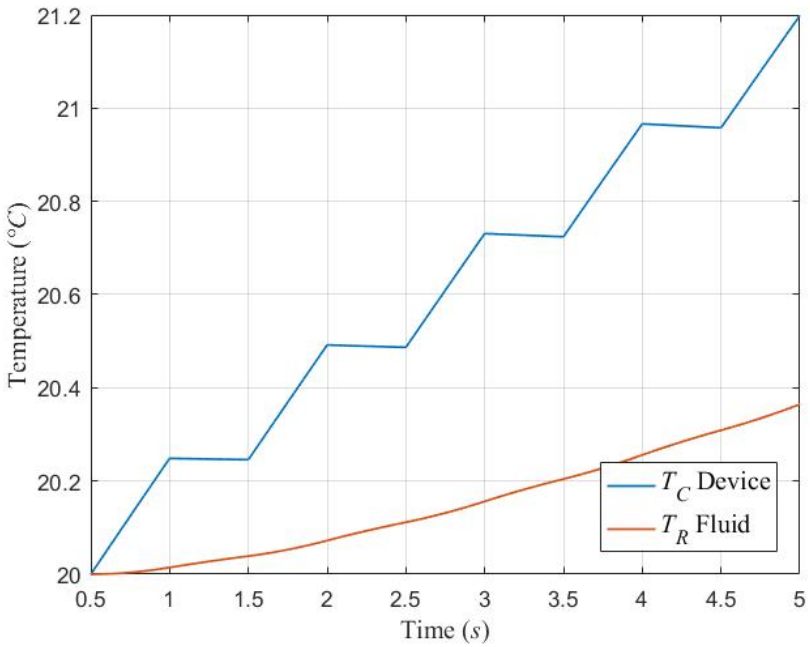

Figure 6. Demonstration of T_C device temperature and T_R return fluid temperature relationship.

Analyzing the thermal resistance of (2) and comparison to the load power, it's possible to understand the dynamic of how the resistance changes over time. Figure 7 shows the increase in resistance during the on period of the pulse. Additionally, the magnitude of increase per pulse is greater than the magnitude of decrease during the off period. During the pulsed off period the fuel is acting to cooling the device. The amount of cooling that takes places is limited given the difference between the device temperature and tank temperature is low.

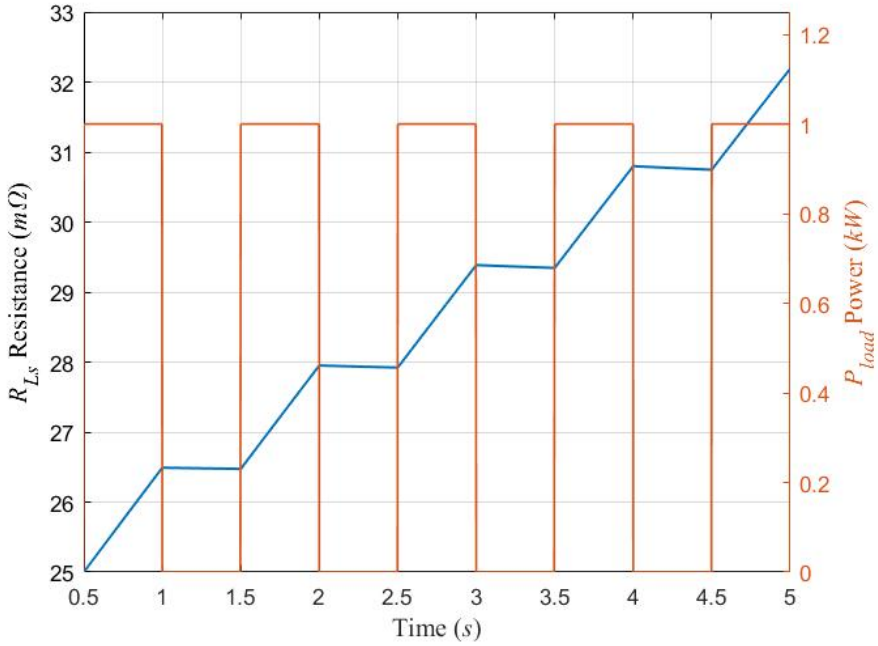

Figure 7. R_{Ls} series resistance v. P_{load} pulse power demonstrating the linear relationship between the pulse load and series resistance.

5 System Stability

5.1 Defining Stability

Experiments show stability issues exist at both low and high T_C device mass temperatures corresponding to the thermal R_{Ls} series resistance. The device temperature is based on the load parameters and required output of the system. It's important to determine the capabilities of the current system and future steps can be taken to improve stability performance. Traditionally, a system is defined to be stable or unstable. Such as an electric motor given a pulsed signal to move a mass a specified distance at a certain frequency. A stable open loop system will move the mass some distance and any transients will be damped out over time. If the motor cannot perform the required operation, it will either oscillate without damping or exceed the motor physical limitations and fault out. With the system studied in this thesis, it has been found that there exist points of operation where the system is unstable, stable, and then unstable. Whenever this operating region is discovered, it is labeled as metastable [12].

To demonstrate this type of stability issue, the pulsed power load is adjusted to 7500 W (P_{load}), pulse period to 1 s (T_P), and duty cycle to 50 % (D_P). Additionally, the phase delay is set to 0.5 s, meaning the pulse load will go high every n.5 s mark (0.5 s, 1.5 s, 2.5 s, etc). At the initial low mass temperature of the weapon, the series thermal resistance is very low and develops a near short to the bus. As the pulsed load goes high and draws current from the source, the bus voltage develops increasing transients, shown in Figure 8. The bus voltage spikes at 580 V which is more than double the nominal voltage.

Conversely, the voltage drops to 0 V before the pulse is turned off. Both conditions constitute a failure of the system.

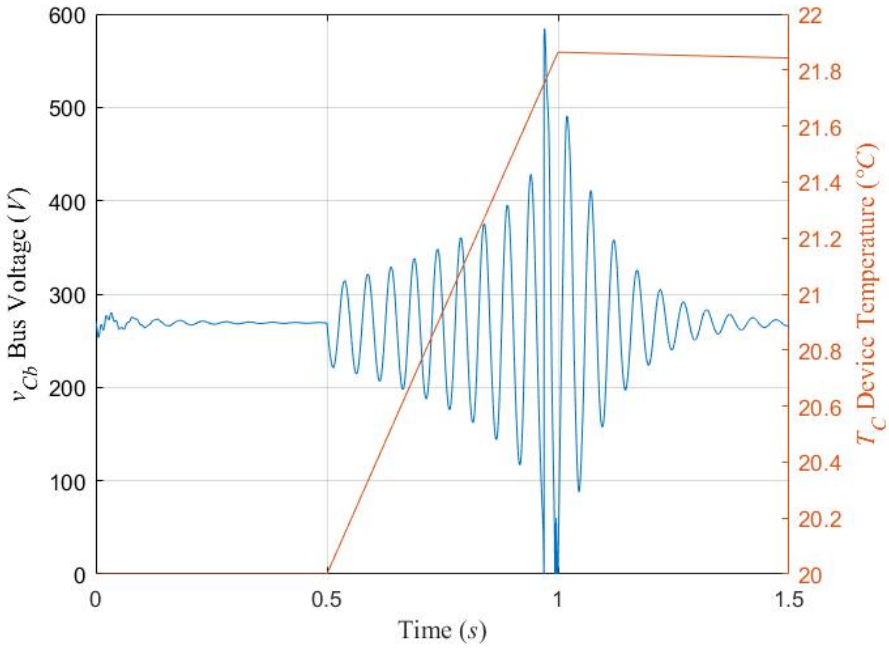

Figure 8. Demonstration of low temperature bus voltage metastability. The bus voltage experiences states of instability during the pulse on period and stability during the pulse off period.

During this first pulse the device begins to immediately heat up from its initial temperature of 20 °C. Following (2) and (3), the thermally coupled R_{Ls} series resistance also begins to increase from its initial value of 25 mΩ. The series resistance coupled with the capacitance of the total load acts as a low pass filter to the electrical bus. The frequency of osculation during the pulsed period is 20 Hz falling below the cutoff range of the filter. As the resistance increases over time with temperature, the filter begins to attenuate these

periodic oscillations. At the end of the first pulse period, the temperature dependent resistance has increased to 35.8 mΩ (a 10.8 mΩ increase).

After several pulse periods, the higher series resistance induces a larger voltage drop to the bus stabilizing the oscillations, shown in Figure 9. Transients exist but the magnitude of the largest oscillation is smaller than what was experienced in the few pulses of the load. The transients in this range are no greater than 50 V and decrease in magnitude with each pulse. This pulse period range is stable as both the pulse on and pulse off period have decreasing transients. The range of resistance values seen starts at 78.4 mΩ and ends at 99.4 mΩ. During this range of operation, the oscillations aren't completely damped out during the pulse on periods. A steady state voltage is reached for the pulse off period demonstrating stability in the system with the same power load.

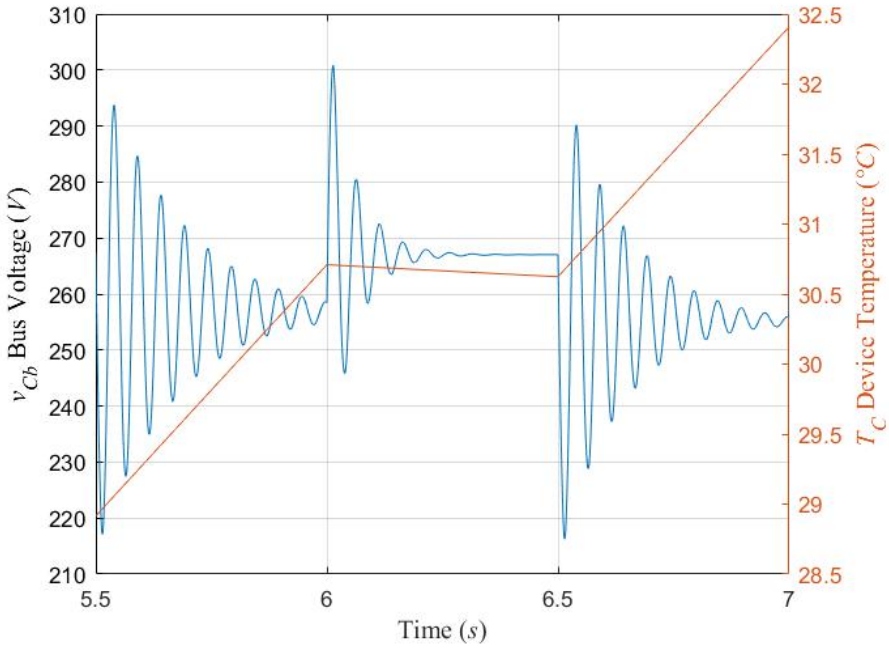

Figure 9. Demonstration of intermediate temperature bus voltage stability. The bus voltage is damped out during the on and off pulsing periods resulting in overall stability.

After several more pulse periods, the device temperature has greatly increased from its initial value, comparing Figure 8 to Figure 10. During the pulsed off period the steady state voltage drop has increased from less than 3 V to 20 V. The resulting R_{Ls} resistance has increased to a range of 563.8 mΩ to 571.6 mΩ. With this high of a resistance value there are no longer any transients that occur during the pulsed on or off periods and only minor overshoot during the pulse on period. A consequence is the voltage drop from the higher series thermal resistance is larger than the main voltage source of the DC grid network. The current demanded by the pulsing power device causes a voltage drop that exceeds 135 V (the supply voltage to the boost converter v_s). At this point the bus voltage begins to collapse (goes to a 0 V value) causing a complete failure of the system.

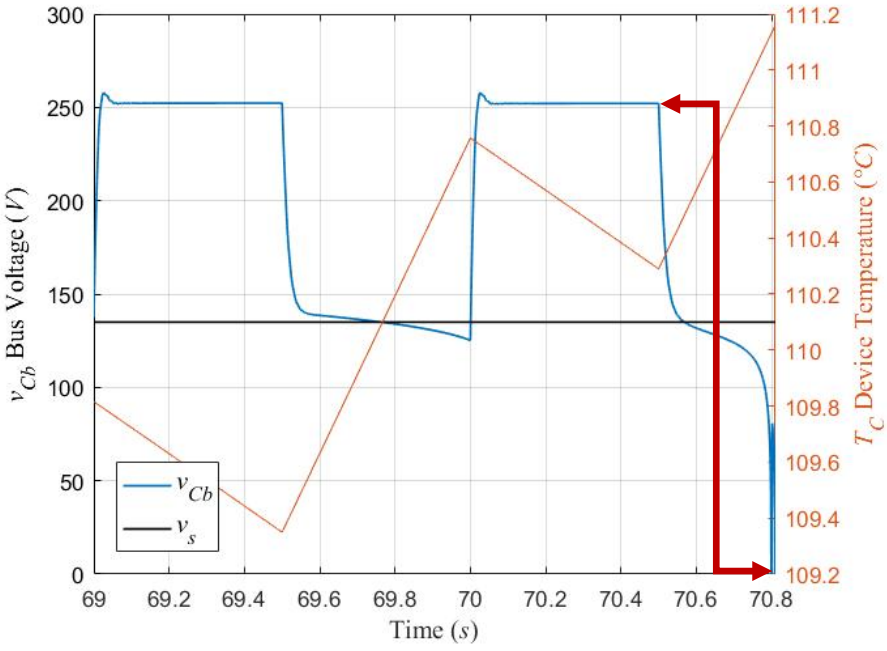

Figure 10. Demonstration of high temperature instability demonstrating collapse of bus voltage. The thermal coupled resistance has caused the bus voltage drop to go to zero, highlighted by the red arrow.

The first 70 s interval of the electrical bus voltage for this load case is shown in Figure 11. Observations show that the transients of the first power pulse are nearly 300 V larger than the second pulse. As the device temperature increases, the effects of the initial pulse are damped out. The consequence of this stability is the steady state error during the pulsed on and off periods increases. This trend continues until the pulse on period voltage drop causes the boost converter to fail. The device temperature has increased from 20 °C to 111 °C and a corresponding series resistance increase from 25 mΩ to 571.6 mΩ. This increase between the two states is linear and expected given (2).

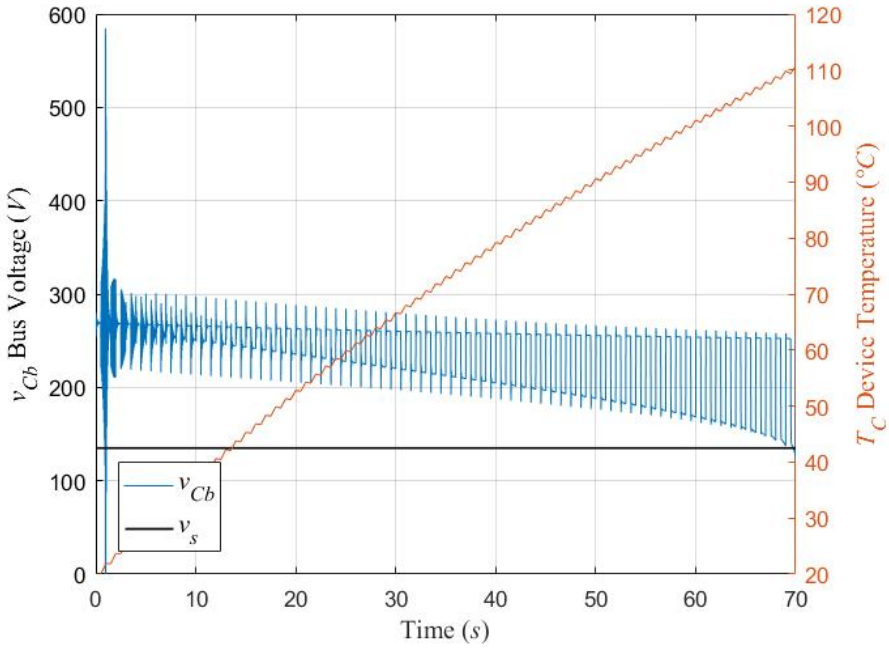

Figure 11. Demonstration of bus voltage over entire test range showing the actual bus voltage v_{Cb} against the supply voltage v_s and device temperature T_C. This shows the non-linear collapse of the bus voltage over time along with periods of stability and instability.

5.2 Mapping Stability Boundary

With the simulation results of chapter 5.1, it is desired to define the operational boundary limits of the system. This is done with thermal and electrical constraints on the EMT model. The boundary focuses on the stability issues of the non-linear model at low and high temperatures. This is done by setting minimum and maximum allowable bus voltage limits for v_{Cb}. The upper voltage limit detects if the system is experiencing low temperature stability issues, having un-damped voltage transients. The lower voltage detects if there are high temperature stability issues, having large voltage drops. The voltages defining upper and lower bounds are set to 350 V and 240 V, respectively, within the MATLAB initialization file.

Determining operational boundary of the system allows the dynamics of the large signal analysis of the pulse power load to be fully encapsulated. The four parameters of the pulsed load are systematically adjusted to properly define the region of operation. The first parameter, pulse period (T_P), defines the width of the PWM signal and is swept from 0.001 s to 1 s in 0.001 s intervals. The second, pulse power (P_{load}), is the magnitude of the pulse power load to the bus. This value is swept from 500 W to 10,000 W in 500 W increments. The third variable, phase delay, is set to half of the pulse period so if there are any startup transients, they do not affect the dynamics of the pulsing power load. The fourth parameter, duty cycle (D_P), is the variable that is sought after to determine the limit of operation. The duty cycle percentage determines that amount of energy that is transferred per pulse of the device.

The model step size is set to 0.00001 s to accommodate for the resolution of the pulse period. Given the simulation time can be up to 60 s, this results in 6,000,000 data points to store to memory per variable. For this reason, the model was stripped of any "log to workspace" blocks and signal scopes. Additionally, the model is run only from memory rather than having the Simulink file open to cut down on total memory use. This is the reasoning by only logging the t_{out} variable and decrease simulation time for the systems deemed unstable.

The program locates this stability boundary by determining the maximum allowable duty cycle (D_P) given a set pulse period (T_P) and pulsed load (P_{load}) and tracking the bus voltage, v_{Cb}. When the v_{Cb} value meets the minimum or maximum threshold limits that are set forth, the simulation is stopped. The Simulink simulation time, t_{out}, is logged to the MATLAB workspace and analyzed after the simulation has either been stopped or

completed. The last recorded simulation time and the desired simulation time values are passed to the comparison function. If the last t_{out} value is less than the listed end time, the simulation is then flagged as unstable.

When the simulation first starts, the duty cycle value starts at 1 % and the pulse period and load magnitude are at their initial values. If the simulation given a load condition is deemed stable, the duty cycle is increased by 1 %. This is done until the simulation is deemed unstable or reaches 100 %. If deemed unstable, the maximum allowable duty cycle is recorded as 1 % less than last used duty cycle. If a duty cycle of 100 % is reached, the maximum duty cycle is recorded as 100 %. This recorded duty cycle is then decreased by 1 % and serves as the starting point for the next pulse period (T_P) keeping P_{load} fixed. This is repeated through the range of period values tested for a fixed power until the entire period range is mapped. The duty cycle is then reset to 1 %, the period is reset to its initial value, and the power load is incremented by one step (500 W). This process repeats itself until a maximum duty cycle is mapped for the entire range of pulse periods and power loads.

5.3 Stability Boundary Hypothesis

Through linear small signal analysis, it is expected that the resultant surface boundary layer will develop a plateau representing maximum power transfer. It is also expected that extending from this plateau there will be a cliff showing a linear relation between maximum power and duty cycle, to a point. It is the expectation that at some point there will be a non-linear relation between the pulse period and maximum allowable duty cycle given a fixed power.

6 Metastable Duty Cycle Surface

Results from methodology of chapter 5.2 are shown in Figure 12. The surface shape of this test begins to validate the hypothesis of 5.3 showing the regions of maximum power transfer (the plateau), partial linear relationship between duty cycle and power load (cliff), and the non-linear relationship between the duty cycle and pulse period (ripples). The area of 100 % duty cycle available can also be labeled as the constant power region. In this region regardless of pulse period or load magnitude, the system will be stable for any duty cycle. All regions under the surface beyond the plateau are labeled as metastable. Different combinations of pulse period, load, and duty cycle will result in either stable or unstable behavior depending on duty cycle.

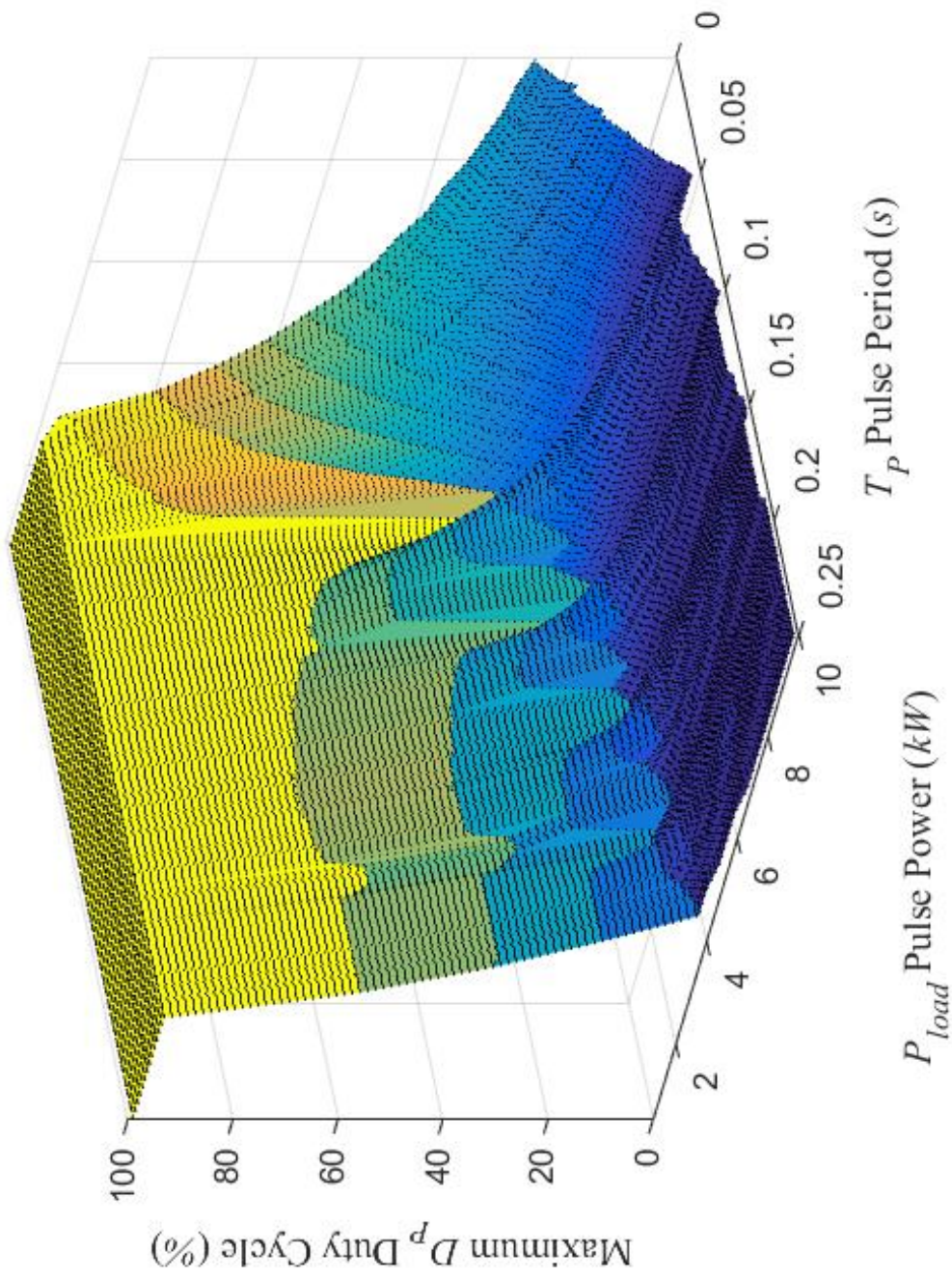

Figure 12. This surface represents the maximum allowable duty cycle with a varying pulsed power load and pule frequency. Regions where the duty cycle is 100 % are labeled stable, the region under the surface as metastable, region above the surface as unstable, and the surface itself as marginally metastable.

The boundary layer between the metastable condition and unstable condition will be labeled as marginally metastable. This is best illustrated in Figure 13 showing one slice of Figure 12 at a given pulse period over the power load range. Given a pulse period, there exists regions of stability, metastability, marginal metastability, and instability. Taking another slice from Figure 12 given a constant power is seen in Figure 13. The results of these figures show that given a power load the system falls into one of two categories. First, the system can be in complete stability where there are no limits to duty cycle given pulse period and power. Second, the system can only have regions of metastability, marginal metastability, or instability given any set of load conditions. It is this condition that is seen in Figure 13. Another slice of the surface is seen in Figure 14. This shows that given a pulse load, the region may only be metastable, marginally metastable, or unstable.

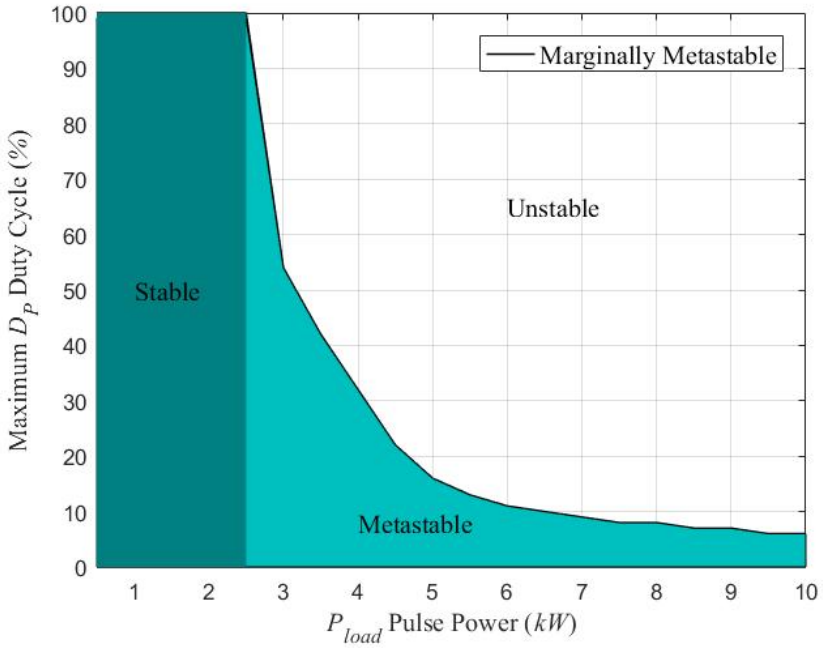

Figure 13. Marginally metastable boundary layer at 0.075 s pulse period over the entire pulse power load range.

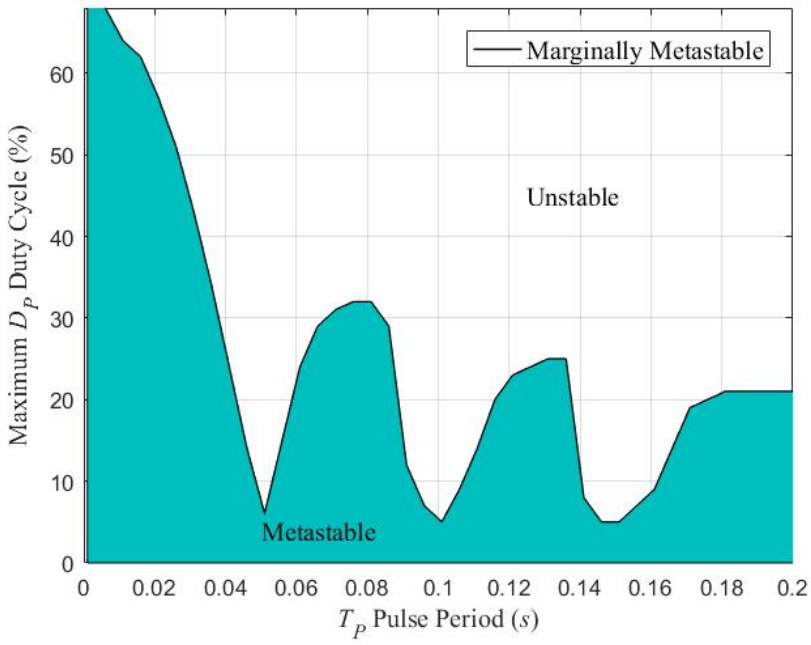

Figure 14. Marginally metastable boundary layer at 4000 W pulse load over region of pulse period lengths.

6.1 Voltage and Thermal Analysis

The first portion of analysis of this surface involves the v_{Cb} bus voltage transients and resultant R_{Ls} thermal series resistance results. Over a portion of Figure 14, three points of equal pulse width are determined in regions of metastability, marginal metastability, and instability. Choosing points of equal pulse width defines each point to expel an equal amount of energy. Restated, each load characteristic is performing the same amount of work but under different operating parameters. These three points chosen are shown in Figure 15.

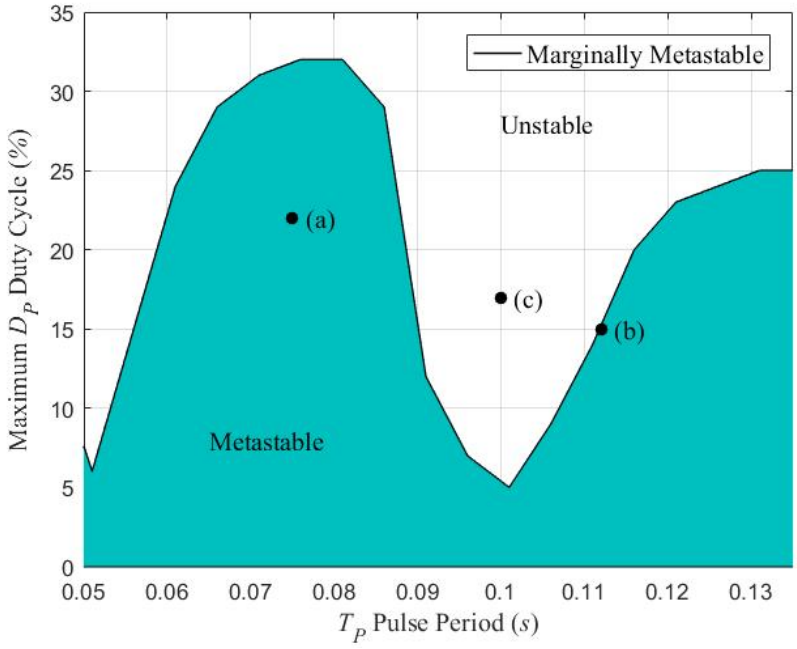

Figure 15. Stability surface slice at 4000 W showing analysis points (a) T_P = 0.075 s, D_P = 22 %; (b) T_P = 0.112 s, D_P = 15 %; (c) T_P = 0.1 s, D_P = 17 %.

The resultant bus voltage transients from these three points are shown in Figures 16 and 17 with the load power over-laid. Figure 16 demonstrates the low device temperature transients. During (a) the bus voltage experiences transients given the pulsing of the device, however these transients aren't completely damped out as steady state voltage isn't reached. The voltage decreases when loaded and then experiences an additional transient when pulsed off. During neither pulsing on or off periods does the voltage reach a steady state value. (b) experiences larger transients than (a) but is still within the allowable system specifications. It is noted that the voltage nearly reaches a steady state value during the off period caused by the cycling of the load. (c) shows the unstable region of the system where

the bus voltage overshoots the minimum and maximum bus voltage boundary. The transients induced by the load remain un-damped with the low thermal resistance of R_{Ls}.

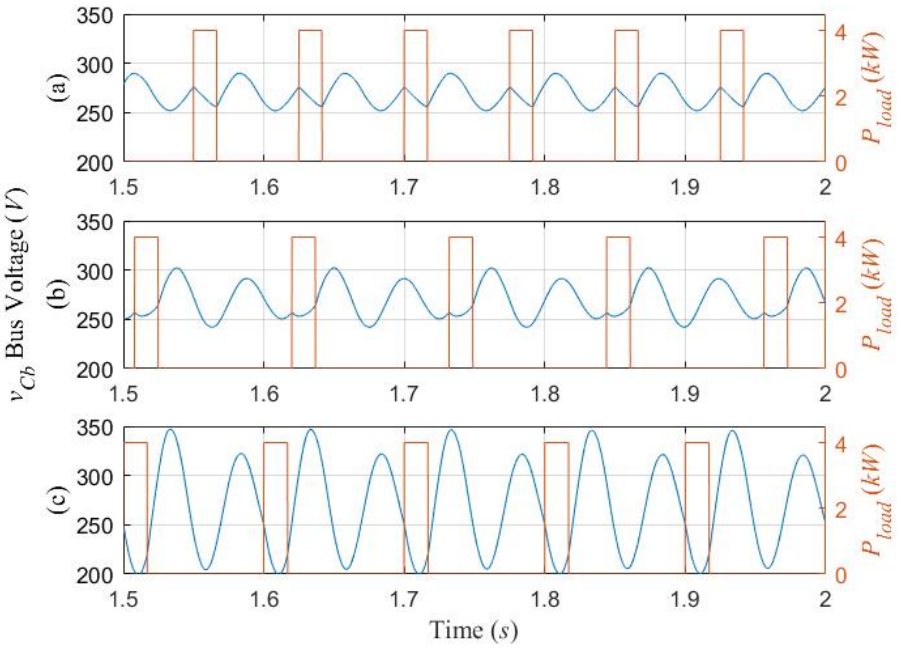

Figure 16. Low T_C temperature v_{Cb} bus voltage analysis at points (a) T_P = 0.075 s, D_P = 22 %; (b) T_P = 0.112 s, D_P = 15 %; (c) T_P = 0.1 s, D_P = 17 %.

High temperature analysis of these three points, shown in Figure 17, yields similar results to Figure 16. Comparison between the low and high temperatures, two notable differences exist. The first is that for all test points, the average value of the waveform has decreased. The device temperature has increased resulting in a higher R_{Ls} series resistance inducing a voltage drop. The second difference is the unstable test condition bus voltage is no longer unstable. The voltage waveforms for all three cases are attempting to damp out the transients but can't due to the pulsing frequency of the load. All three cases experience

stability given the transients are in the process of being mitigated before the next pulse occurs.

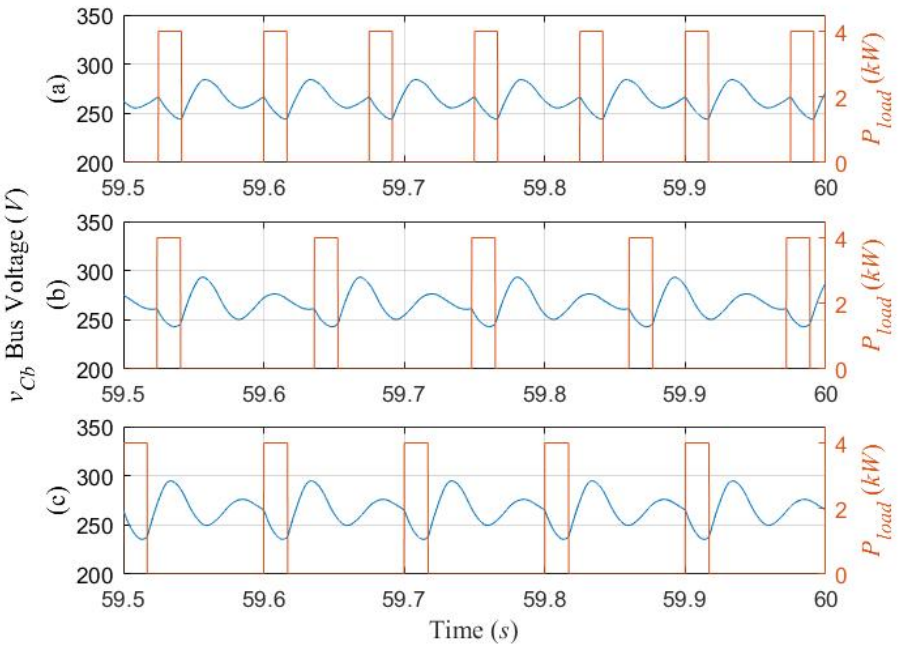

Figure 17. High T_C temperature v_{Cb} bus voltage analysis at (a) T_P = 0.075 s, D_P = 22 %; (b) T_P = 0.112 s, D_P = 15 %; (c) T_P = 0.1 s, D_P = 17 %.

Demonstrating the perturbation of the system of the R_{Ls} thermal resistance, Figure 18 shows the resultant dynamic resistances. The first observation is the metastable system experiences the highest operating series resistance compared to the marginally metastable and unstable system. Another observation is the marginally metastable resistance has the smallest end value and lowest trajectory. Interpretation of these figures show the marginally metastable test case as the most efficient path for the system to operate. The lower series resistance implies that operating on this boundary layer the system experiences

less resistive power loss. This results in more source energy can be expended into the device as well as the pump motor for cooling and thermal management.

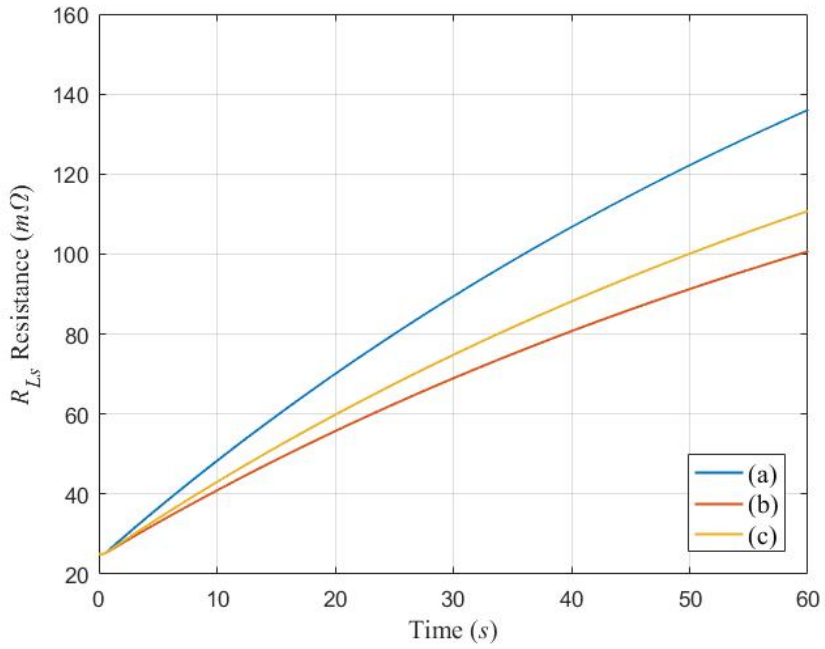

Figure 18. R_{Ls} thermally coupled series resistance at (a) T_P = 0.075 s, D_P = 22 %; (b) T_P = 0.112 s, D_P = 15 %; (c) T_P = 0.1 s, D_P = 17 %.

This relationship of the thermal series resistance between the three test cases is seen in both the weapon mass and return fluid temperatures, T_C and T_R respectively. Figures 19 and 20 show the temperature relation at each test case of metastability, marginal metastability, and instability of the device and return fluid. This demonstrates the marginal metastable test case offers better cooling performance over the metastable condition. The device and coolant temperatures have a 6 °C and 3 °C cooling performance increase with the marginally metastable compared to the metastable test. This cooling enhancement is

related to the series resistance corresponding to the PMDC machine supply voltage. Given there is a lesser voltage drop and deviations to the bus as compared to the metastable and unstable conditions, the motor can pump more coolant thusly better cooling the system.

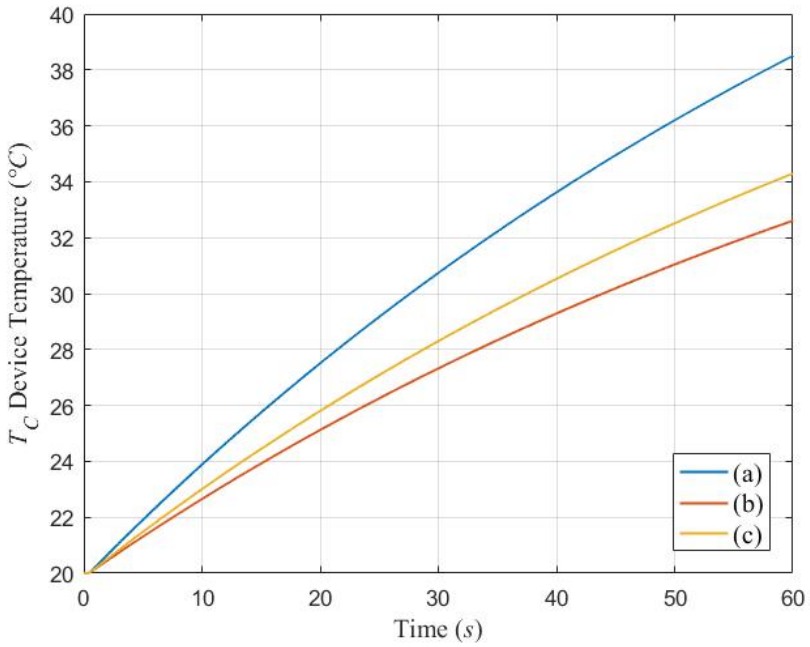

Figure 19. T_C device temperature at (a) T_P = 0.075 s, D_P = 22 %; (b) T_P = 0.111 s, D_P = 15 %; (c) T_P = 0.1 s, D_P = 17 %.

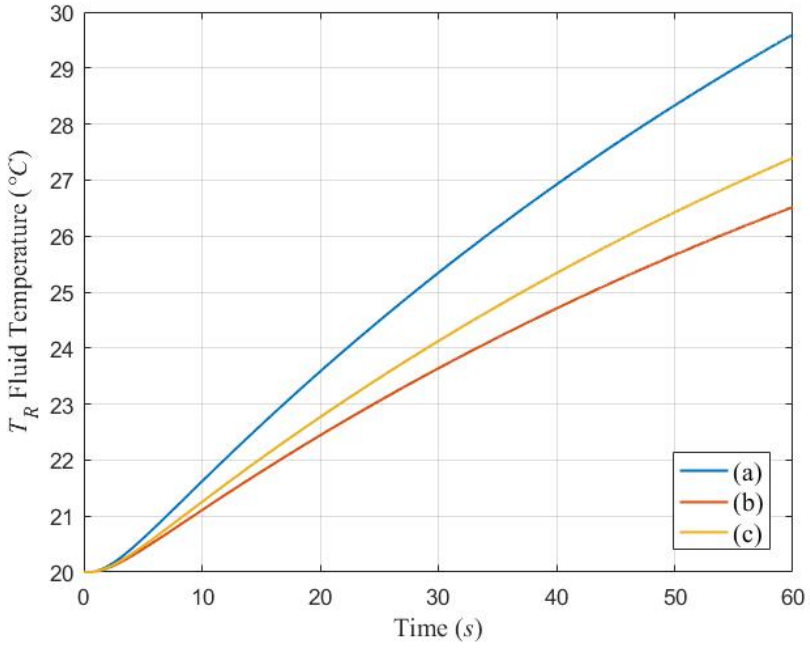

Figure 20. T_R return fluid temperature at (a) T_P =0.075 s, D_P = 22 %; (b) T_P = 0.111 s, D_P = 15 %; (c) T_P = 0.1 s, D_P = 17 %.

The low temperature summary is shown in Table 4, which is the same 0.5 s interval seen in Figure 16. It's seen that the unstable condition bus voltage transients are nearly five times larger than the stable condition. During this startup region, the T_C device temperature and R_{Ls} series resistance values are all very close together and no real conclusions can be drawn. The pulsing frequency of the load causes the large bus voltage transients of the unstable condition given the pulsed frequency is exactly half the resonant frequency. The metastable and marginally metastable conditions have frequency's that are either slightly above or below 10 Hz. This shows that during the low temperature region it's best to operate the system at frequencies that are different multiples of the resonant frequency.

Table 4. Low Device Temperature Voltage Test Summary

	Metastable	Marginally Metastable	Unstable
v_{Cb} Transient *(V)*	37	60	143
Maximum T_C (°C)	20.9	20.6	20.7
Maximum R_{Ls} (mΩ)	30.2	28.6	29.0

The summary of the high temperature comparison is seen in Table 5, which is over the same 0.5 s interval seen in Figure 17. These results show that the transients of the unstable and marginally metastable conditions have improved. The transients of the metastable condition have increased slightly over the low temperature regions. The marginally metastable T_C device temperature is 6 °C cooler and the R_{Ls} resistance is 35 mΩ less than metastable condition. This shows that the marginally metastable condition has the best thermal operating characteristics, even though the metastable condition has smaller bus voltage transients. These results also show that the frequency of the pulsed load has a larger impact on the system during the low temperature regions.

Table 5. High Device Temperature Voltage Test Summary

	Metastable	Marginally Metastable	Unstable
v_{Cb} Transient *(V)*	40	50	59
Maximum T_C (°C)	38.6	32.7	34.4
Maximum R_{Ls} (mΩ)	136.7	101.1	111.2

7 System Pulse Energy and Average Power

The goal of a DEW system or any pulsed power system is to deliver the maximum amount of energy from the device into the target of interest. Taking the marginally metastable surface of Figure 12, the pulse energy is calculated and shown in Figure 21. Three noticeable differences of the pulse energy surface compared to the duty cycle exist. First, the pulse energy ripples have a smaller overall magnitude. Second, given any range of test values a global maximum per pulse energy exists. Lastly, the global maximum of pulse energy lies on a linear plane that defines the plateau of the duty cycle surface. This slope is directly correlated to the pulse period of the load. The longer the pulse period, the longer the pulse on period of the device.

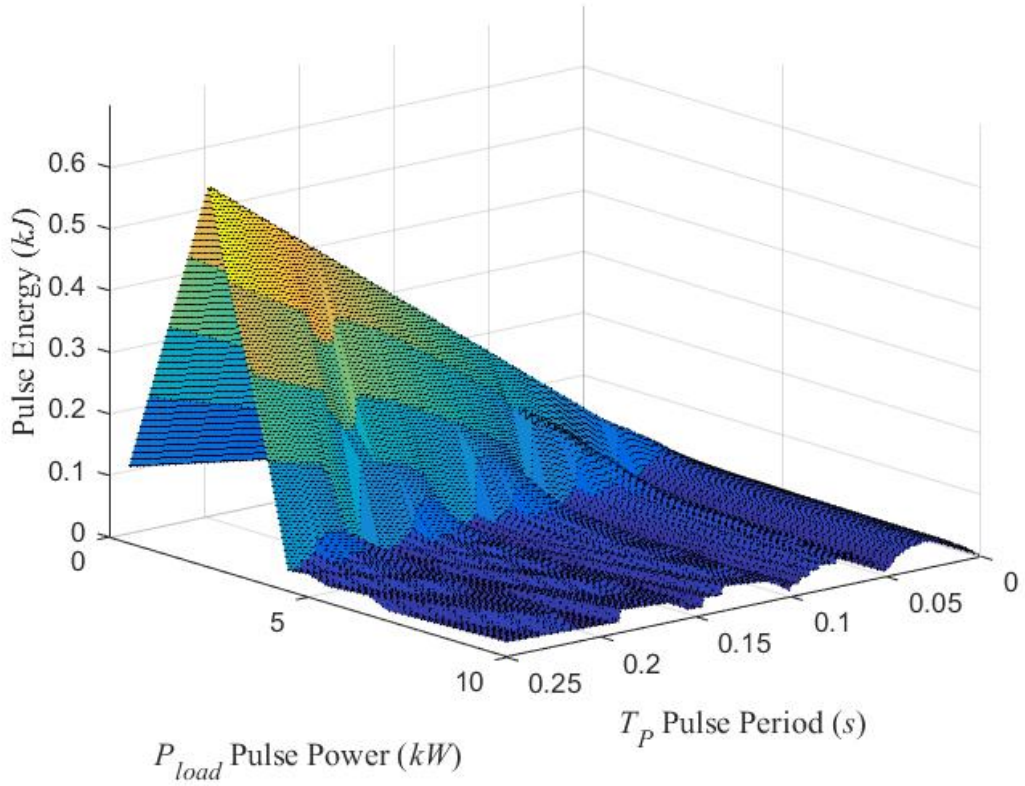

Figure 21. Maximum per pulse energy output of system over marginally metastable surface boundary layer.

The pulse energy surface shows the energy per pulse that can be transferred from the system to a specific target. An extension of the per pulse energy output is the time average power output from the system. The average power is calculated by multiplying the maximum duty cycle by pulse power magnitude. Figure 22 shows the results from this process by defining a new surface boundary. It is noted that the same ridge exists here as with the pulse energy surface plot. A key difference between the two is that at low pulse periods, the average pulse power exhibits local maximums.

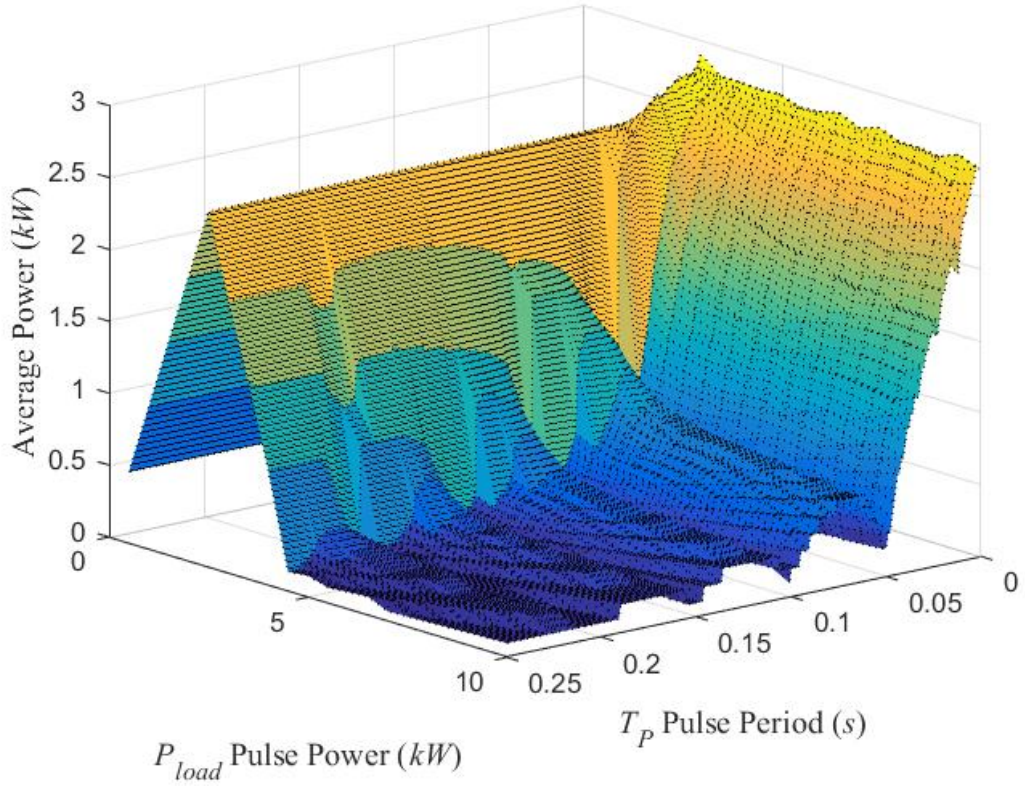

Figure 22. Maximum average power output of system over marginally metastable surface boundary layer.

7.1 Average Power and Thermal Analysis

The surface plots of Figures 21 and 22 allow for analysis to look at the peak pulse energy of the system compared to equivalent average power output at other pulse period, duty cycle, and amplitudes. Three points are chosen for analysis based on power load and average power. The first point is at the peak pulse energy (PPE) output of the system, representing maximum per pulse energy output. The second point has the equivalent load power (P_{load}) but at a higher frequency (lower T_P value) than the PPE, keeping an equivalent average power output (EPHF). The third test point has an equivalent average

power as the first two points but a higher pulse power (P_{load}) while keeping the higher frequency (HPHF). These test points and corresponding parameters are quantified in the following table.

Table 6. Test Conditions

	PPE	**EPHF**	**HPHF**
T_P Pulse Period (ms)	250	8	8
P_{load} Pulse Power (W)	2500	2500	7500
D_P Duty Cycle (%)	99	99	33
Pulse Energy (J)	619	20	20
Average Power (kW)	2.475	2.475	2.475

Figure 23 enhances Figure 22 allowing each test condition to be visualized on the average power surface. This figure gives a better representation that each of the points are in the same plane of average power while on the marginal metastable boundary layer. This comparison demonstrates the effectiveness of implementing the device at a higher pulse power and low frequency versus the low pulse power and high frequency.

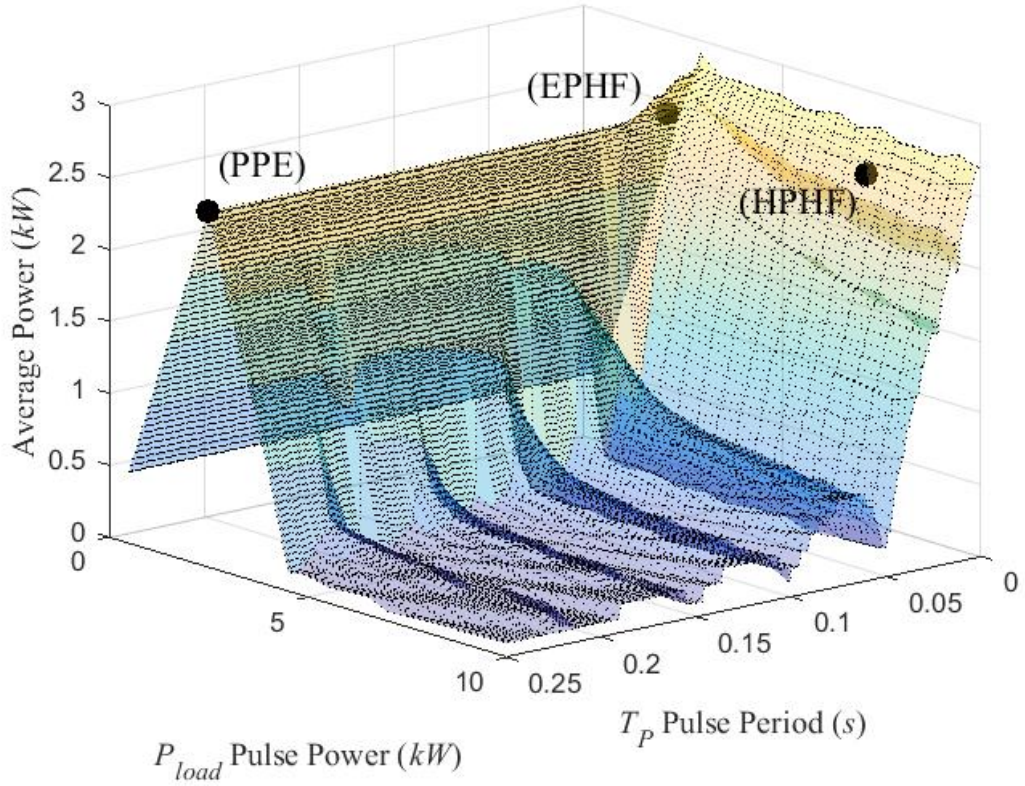

Figure 23. Average power points for T_C temperature, v_{Cb} bus voltage, and R_{Ls} thermal resistance analysis. This visual representation shows the three points are in the same plane.

Figure 24 shows the bus voltage of the system compared over four pulses of the simulation at each test point. This test represents the low temperature simulation as the device is starting from initial conditions. These results show the PPE has higher bus voltage transients caused by the longer pulse period coupled with lower R_{Ls} series resistance. The maximum PPE transients measure 12 V. The HPHF transients are sawtooth in nature and measure to be 12 V. The EPHF test case experiences no transients as compared to the PPE and HPHF tests, even with no active control on the source boost converter.

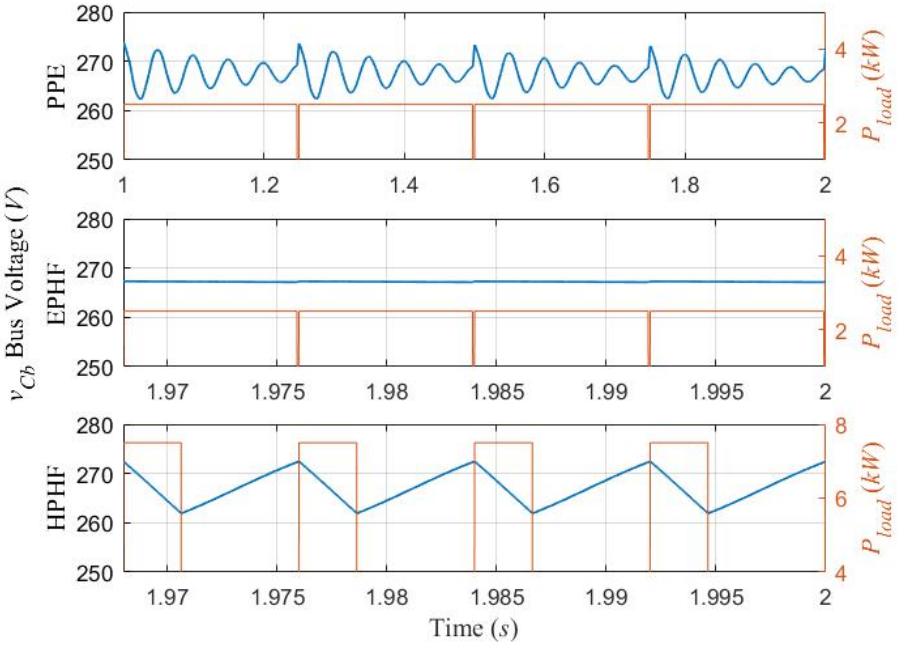

Figure 24. Low T_C temperature v_{Cb} comparison over the last four pulse periods during the first 2 s of the simulation at points of PPE, EPHF, and HPHF.

The corresponding device temperatures are shown in Figure 25 demonstrating the thermal dynamics during the last 32 ms of the first 2 s test period. The temperatures in each test case have the same linear trend upwards and are within 0.01 °C of each other at any given point during the low temperature startup region. The PPE and EPHF tests have no transients while the HPHF test has relatively large transients of 0.01 °C. Figure 25 shows the same comparison of the T_C and Figure 26 R_{Ls} series resistance. Intuitively, the same trends occur as the series resistance is linearly related to the device temperature per Equation (2). Table 7 summarizes the results of the high temperature tests for bus voltage, device temperature, and series resistance.

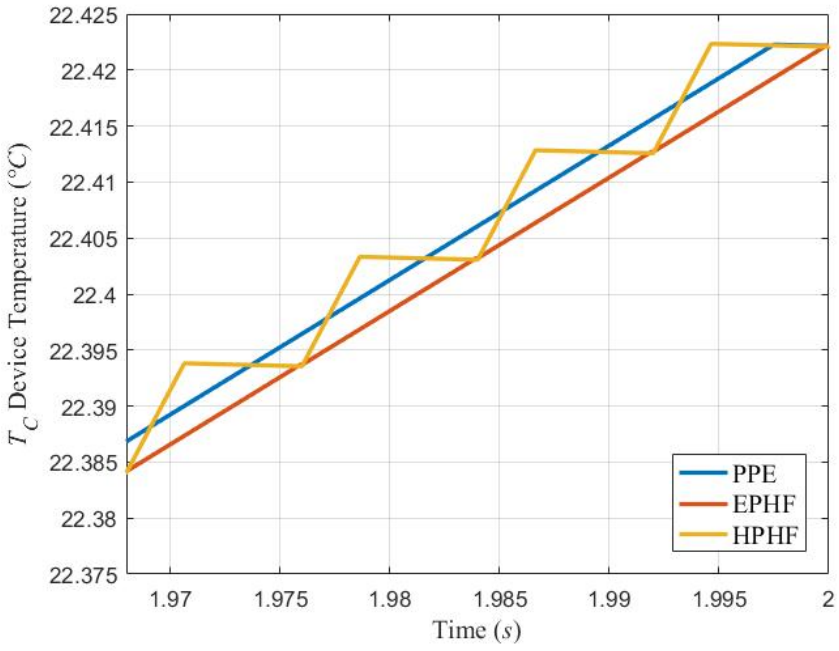

Figure 25. Low T_C temperature comparison over the last four pulse periods during the first 2 s of the simulation at points of PPE, EPHF, and HPHF.

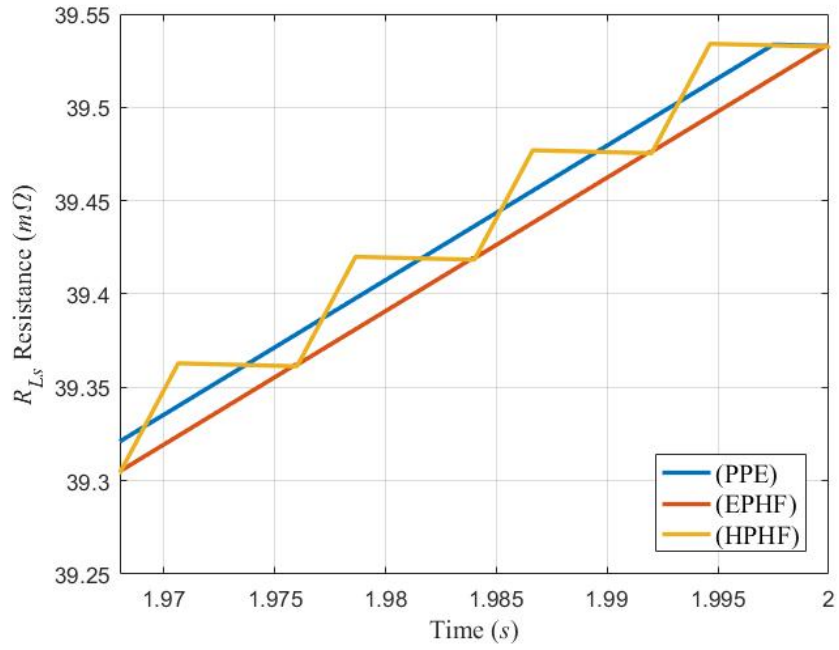

Figure 26. Low T_C temperature R_{Ls} comparison over the last four pulse periods during the first 2 s of the simulation at points of PPE, EPHF, and HPHF.

Table 7. Low Device Temperature Average Power Test Summary

	PPE	EPHF	HPHF
v_{Cb} **Steady State (*V*)**	-	267	-
v_{Cb} **Transient (*V*)**	12	0	10
v_{Cb} **Average (*V*)**	267	267	267
T_C **Final Value (°*C*)**	22.4	22.4	22.4
R_{Ls} **Final Value (Ω)**	0.0395	0.0395	0.0395

The same comparison of the bus voltage, device temperatures, and series resistance are performed at the higher T_C temperatures. The bus voltages shown in Figure 27 are of the last four pulse periods of the simulation (leading up to 60 s). There are two primary differences between this figure and Figure 24. The first is the transients of the PPE test case are much smaller than that of the low temperature case. The high temperature transients yield a magnitude of 5 V with a steady state value of 246 V. The second is the average value for all three cases has reduced to 246 V.

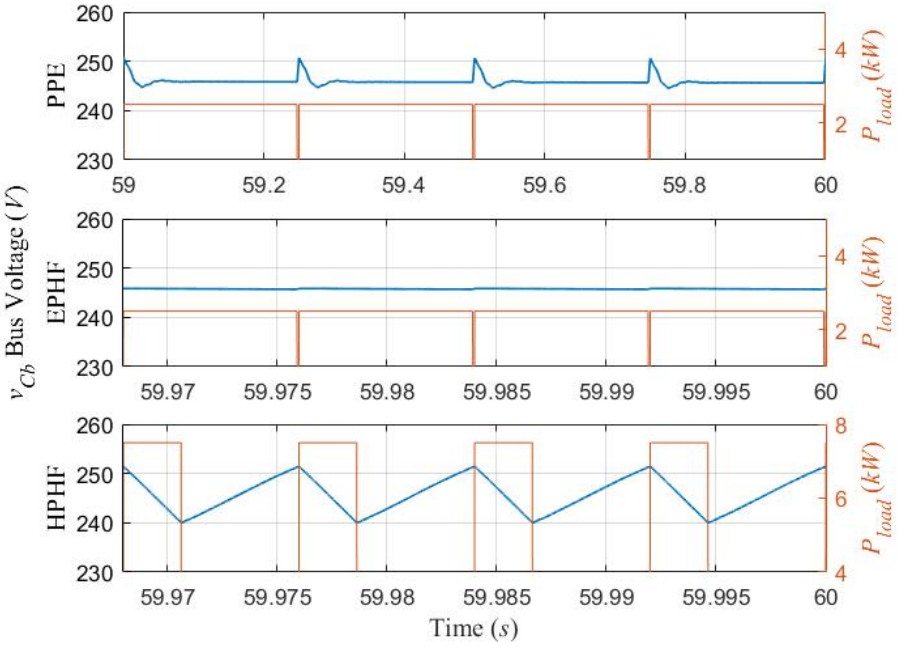

Figure 27. High T_C temperature v_{Cb} bus voltage comparison over the last four pulse periods of the simulation at points of PPE, EPHF, and HPHF.

Figures 28 and 29 show the corresponding high device temperature and series resistance values. The results show that for all three test cases, both states experience the same upward trends and deviations between anyone test case are small. The HPHF test case again have the largest singular transients of the three test cases. Table 8 summarizes the results of the high temperature tests for bus voltage, device temperature, and series resistance.

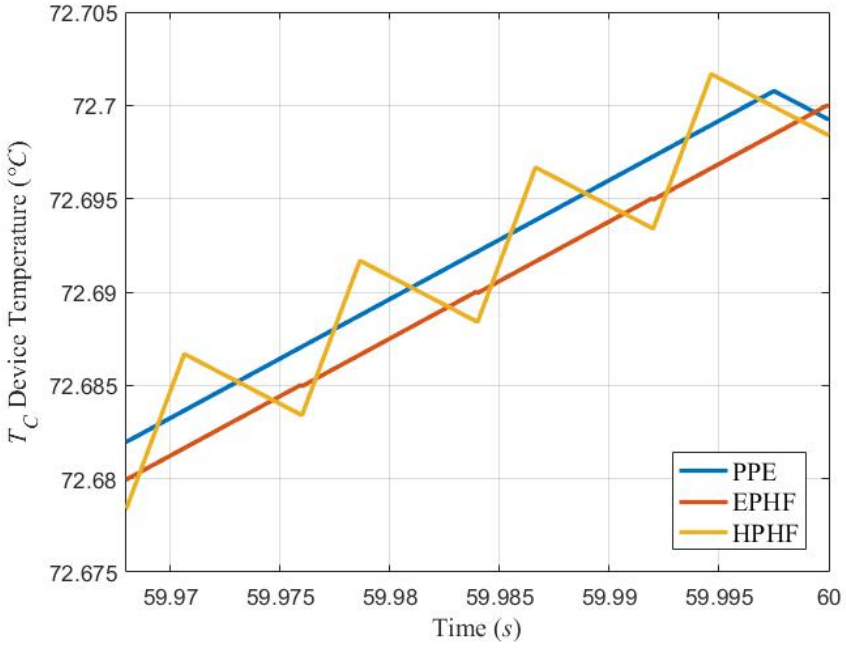

Figure 28. High T_C temperature comparison over the last four pulse periods of the simulation at points of PPE, EPHF, and HPHF.

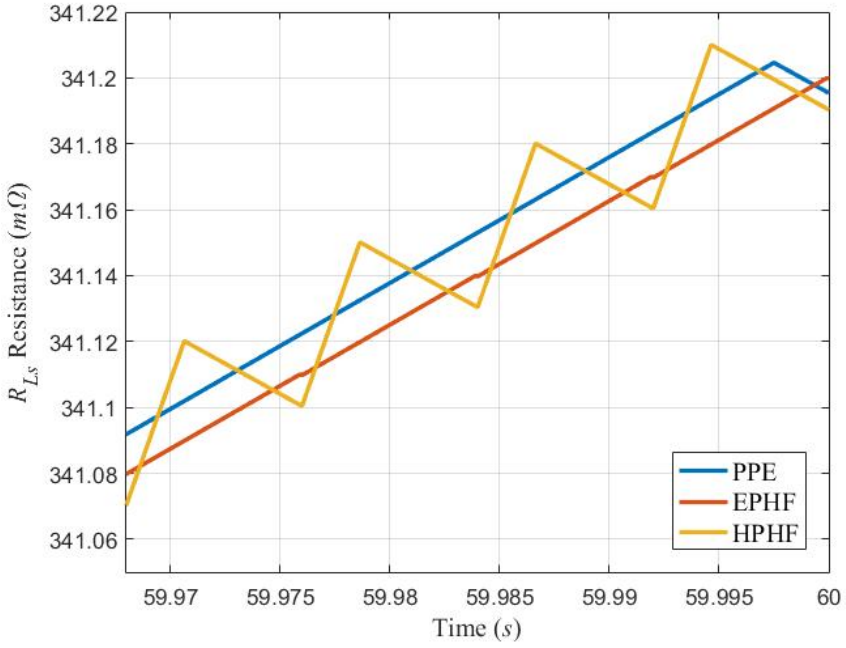

Figure 29. High T_C temperature R_{Ls} series resistance comparison over the last four pulse periods of the simulation at points of PPE, EPHF, and HPHF.

Table 8. High Device Temperature Average Power Test Summary

	PPE	EPHF	HPHF
v_{Cb} **Steady State (*V*)**	246	246	-
v_{Cb} **Transient (*V*)**	5	0	10
v_{Cb} **Average (*V*)**	246	246	246
T_C **Final Value (°C)**	72.7	72.7	72.7
R_{Ls} **Final Value (Ω)**	0.3412	0.3412	0.3412

These results show with a higher frequency load, the effects of the pulse on the bus voltage are mitigated and damped faster compared to a low frequency pulse. Another note is that the device is still heating up and has yet to reach a steady state temperature after one minute of operation. The primary results from these tests have shown that the relationship between average power correlates to the thermally coupled series resistance and device temperature. Using the defined duty cycles in Figure 12, the device temperature is mapped in Figure 30. This more accurately depicts the linear relationship between the average power output of the system and the device temperature. The temperatures shown are the last recorded temperature of from the simulation over the 60 s period. This figure shows that the maximum allowable device temperature is a function of the pulse period as well as the pulse power.

Additionally, this figure demonstrates that the device will remain within required temperature specifications. The results of chapter 6 and equations of chapter 3 demonstrates that the fluid temperature will always be less than that the device temperature given the thermal storage of the fuel tank. The device is the only heat input to the fuel and the fluid in the tank is constantly acting to cool the returning fluid. This shows that the

return fluid will remain under the maximum allowable temperature for JP8 fuel without additives.

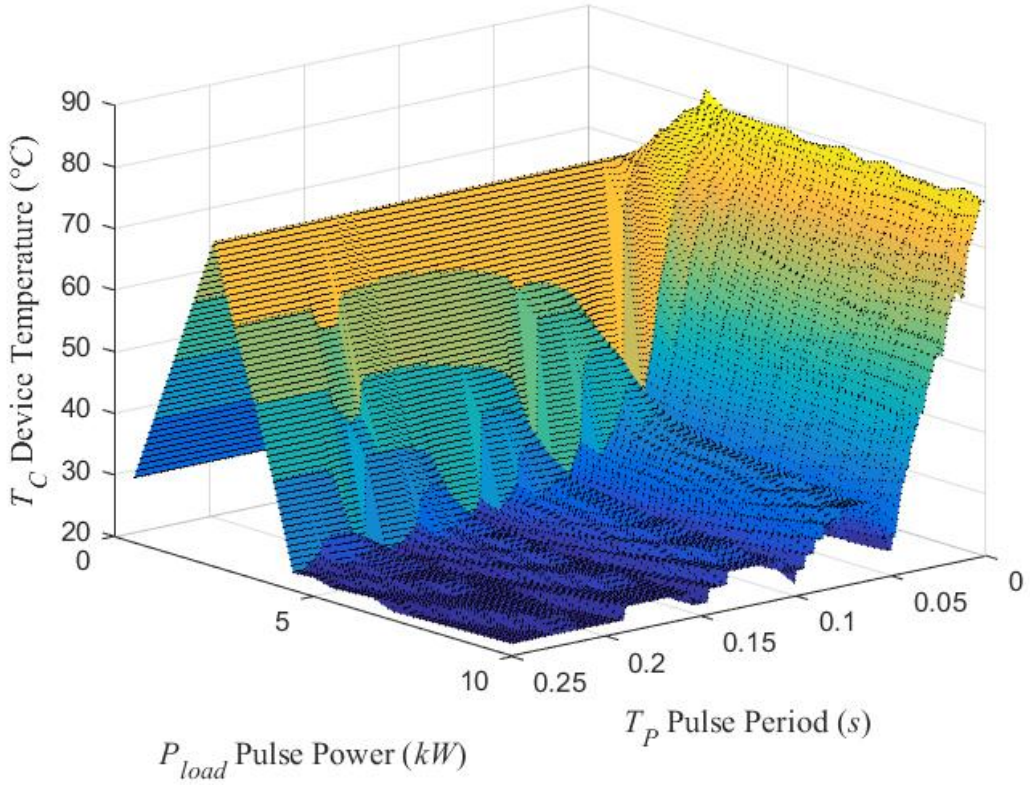

Figure 30. Final T_C device temperature values over the marginally metastable surface.

Using Figure 30 and equation (2), the R_{Ls} series resistance can be calculated. Figure 31 shows the resultant marginally metastable surface plot of the thermally coupled surface resistance following the linear equation of (2), this result is just a scaled variant of the device temperature, demonstrating the maximum series resistance given any load parameters. This correlation better depicts that the maximum allowable series resistance is based on the load conditions of the pulsed device. This figure shows that the maximum allowable series resistance is a function of the pulse period as well as the pulse power.

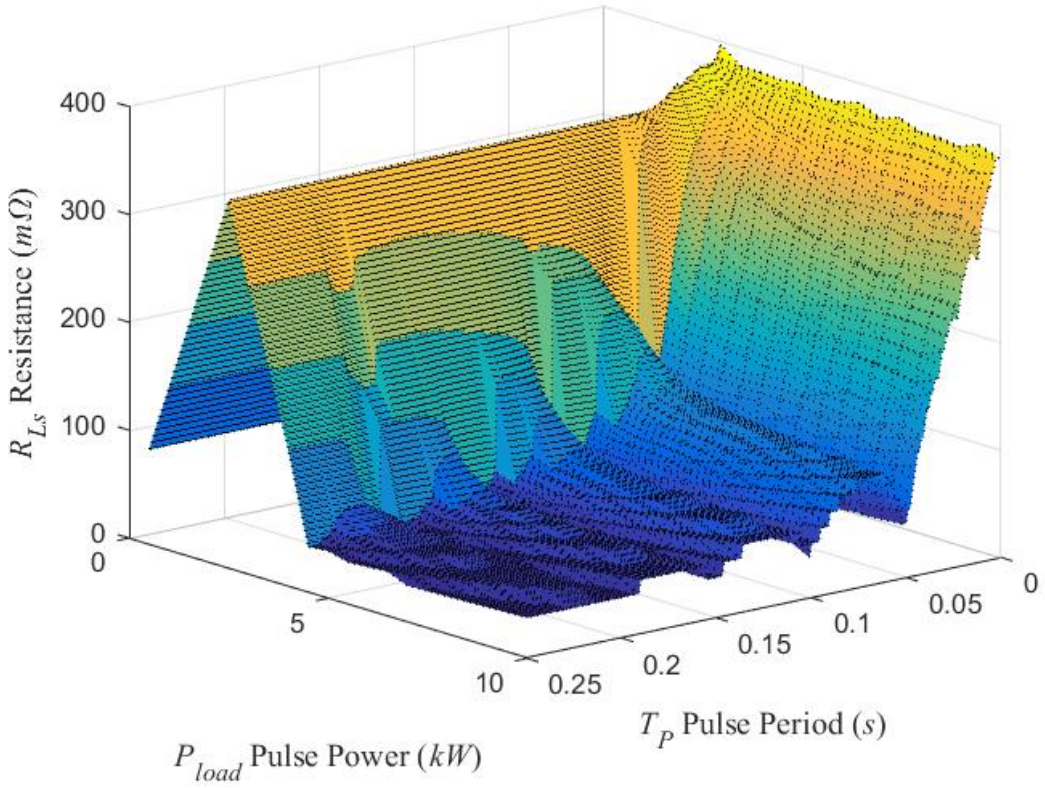

Figure 31. Thermally coupled R_{Ls} resistance final value for the simulation over the marginally metastable surface.

8 Mechanical Analysis

An additional point of focus of the system is the mass of fluid pumped and resultant mass flow rate of coolant through the device. The total mass of fluid pumped through the device during a 60 s interval over the marginally metastable duty cycle surface is seen in Figure 32. This result is found by integration of the mechanical pump speed scaled by the pumping coefficient α_m. This coefficient scaled by the time varying pump speed will result in the mass flow rate of coolant. The mass flow rate of coolant is proportional the amount of cooling power available to the device. It's seen that this surface is inversed to that is seen in the average power marginally metastable surface. This shows that the more power and energy supplied to the device, less power is available to drive the pump motor.

The pump motor buck converter has a fixed duty cycle control of 50 %. This correlates the voltage supplied to the PMDC machine is directly proportional (50 %) to the v_{Cb} bus voltage. There is less than a 9 kg difference between maximum coolant moved and minimum coolant moved. This result of this surface reveals an average mass flowrate of 2.2 kg/s during operation. This flowrate can be viewed as the minimum amount of fluid that is moved during any point of operating the device. It may be possible to adjust the power usage of the pump motor to offset the transients caused by the device pulsed power. This would allow the device to operate at regions of higher power output than what was seen in this thesis. It may also be possible to improve cooling performance of the device and lower power losses caused by the thermally coupled series resistance.

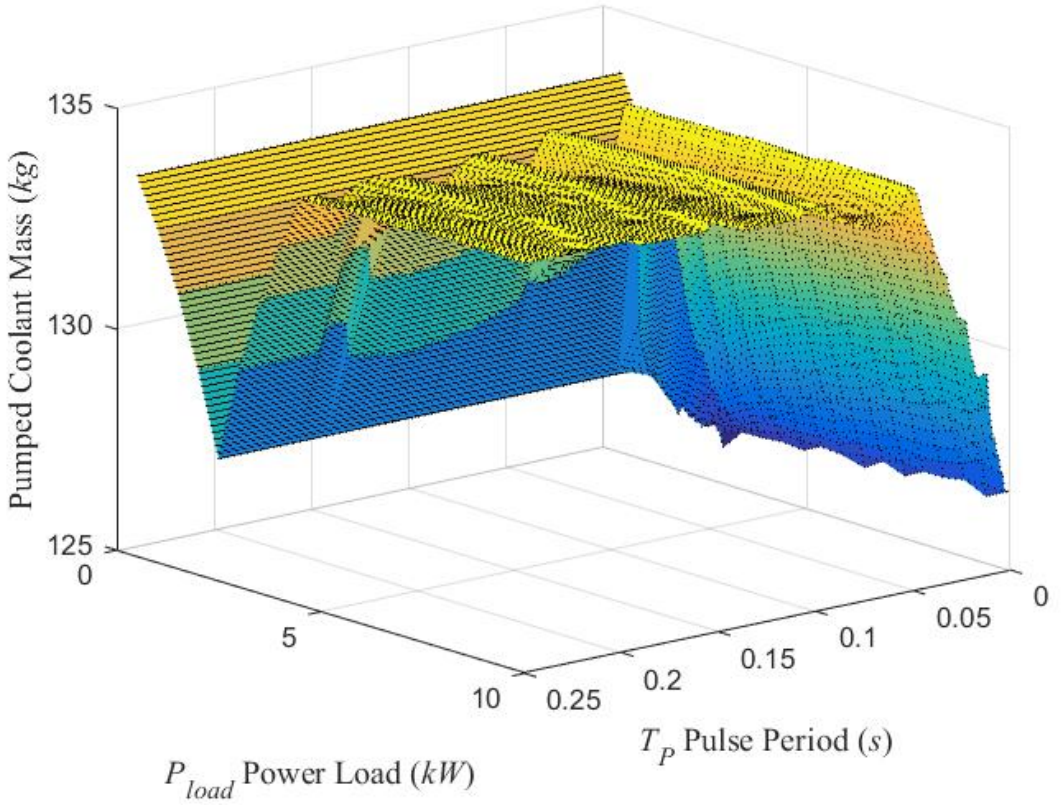

Figure 32. Total mass of coolant pumped through the device during the 60 s simulation period.

9 Conclusion

The results from this thesis demonstrates that there are compounding non-linear stability issues that are caused by the perturbations of EMT system as well as the pulsing power load. The focus is to demonstrate the thermally dependent series resistance and the pulse power load large signal analysis effects on system stability. The combination of these two elements has demonstrated that under different operating conditions the system can be stable, unstable, metastable, or marginally metastable. These conditions are directly linked to the load characteristics of the pulsing device and the thermally coupled resistance.

The system develops stability issues at low and high T_C device temperatures depending on the magnitude (P_{load}) and pulse frequency (T_P) of the load. The low temperature stability issue test demonstrates the transients of the bus voltage increasing without bounds. The high temperature stability issue test shows the pulsed current and thermally coupled resistance developing a voltage drop that can exceed the input supply voltage (v_s). The simulation tool was programmed to first mitigate low temperature stability issues and then address the high temperature stability issues. This process was completed through programmatically cycling all four parameters of the pulse power load. If the system were to experience low temperature transients that exceeded the boundary, the duty cycle was reduced so the device will only develop high temperature stability issues. When the simulation was able to complete the entire 60 s period without the bus voltage dropping below the minimum threshold, it was deemed stable. If at any point there is a desire to run the device longer than a 60 s interval, then additional analysis will need to take place.

Results in chapters 6 and 7 demonstrate that with boundary conditions placed on the bus voltage for minimum and maximum allowable values, the device temperature and fuel temperatures remain within specification. This experiment is performed assuming the device and fluid temperature are equal and relatively low. If either have temperatures above the listed initial conditions, the performance of the system will be different than what is seen in this thesis. If the device is preheated to a certain temperature, it may be possible to mitigate the low temperature stability issues as explained in chapter 5. This could potentially allow the device to operate at a higher power output than the listed maximum.

While running the device with a set pulse period, magnitude, and duty cycle, it's possible to find regions with no noticeable transients. Chapter 7 shows the device will induce smaller transients on the bus if the power is low and pulse frequency is above 20 Hz. Additionally, the closer the operating point of the system is to the boundary layer, the more efficient the device will operate. This will allow for the device to operate cooler as well as put proportionally less heat into the fuel. Having one device add only a small amount of heat would allow for additional equipment to be in a cooling loop. This then relates to the idea of using a device to preheat another device to help mitigate low temperature stability issues.

The average power output of the system is linearly correlated to the device temperature as per (3) and thermally coupled resistance as per (2). This relationship allows for the estimation of the value of temperature given a resistance or measured voltage drop if there is no allowable way to measure the device temperature. This is important if there is no reliable or cost-effective way to measure temperature of the device. Measurement of the

fluid is not an accurate estimation as there is a non-linear relationship between the fluid temperature and the device temperature.

Through average power, energy, voltage, and thermal analysis, it's possible to depict the most efficient area to operate the system at. Considering bus voltage and thermal requirements, the optimal region to operate the system is at a pulse frequency higher than that of the resonant frequency of the system. This ensures that the voltage transients are low given a lower power load or that the harmonics of the pulse help to control the bus voltage at a high-power load. With a pulse load at a high enough frequency, it may be possible to operate the system without any control on the source, reducing complexity of the physical system. This would only be possible if any transients that exist are within an allowable range for other devices on the bus.

Lastly, the results of the study of this non-linear system will aid in the development of Lyapunov based control and analysis of the EMT system. Lyapunov equations are a common tool used in non-linear systems that describe the amount of energy in a given system. From these results, it's possible to view the amount of allowable output energy given any load conditions. The results would help to define the region for each variable in the Lyapunov control workspace. The results will ultimately aid in the development of HSSPFC analysis of the system and development of an overall control strategy.

10 Future Work and Considerations

Continuing this work, it would be desirable to perform more frequency-specific analysis on the pulsing load. This experiment adjusts the pulse period in 0.001 s intervals from 0.001 s to 1 s. This method allows for fast simulation iterations and model implementation to take place but has drawbacks. The following figure shows a portion of a histogram plot of the tested frequencies.

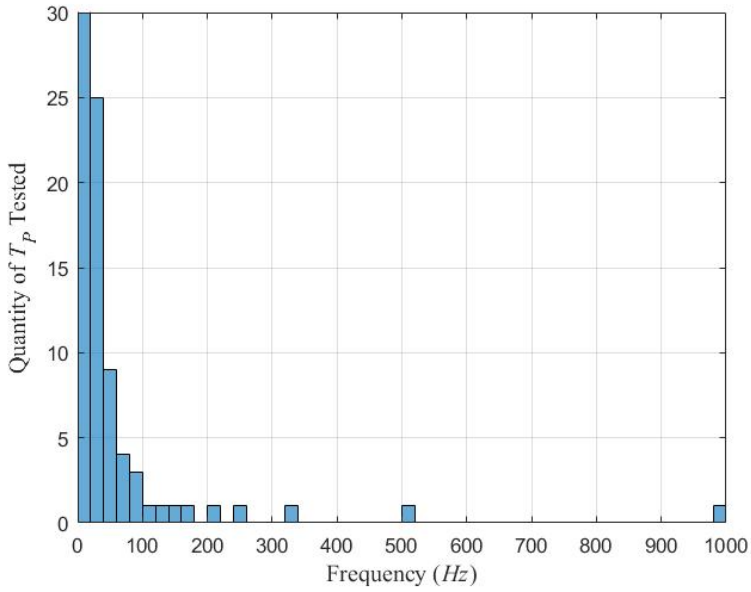

Figure 33. Range of tested pulse frequency (varying T_P) for development of marginally metastable boundary surface.

It's seen that the range of tested frequencies is not linear as is primarily focused on frequencies under 20 Hz. The main portion of non-linear instability stems from tested frequencies above the 20 Hz resonant frequency. It would be desirable to analyze the system at specific PWM frequencies rather than specific pulse periods, such as in 10 Hz increments from 20 Hz up to 1000 Hz. It then maybe possible to better explain the relationship between the pulsing frequency and the system's natural frequency.

11 Reference List

[1] H. Ebrahimi, H. El-Kishky, M. Biswass, and M. Robinson, "Impact of pulsed power loads on advanced aircraft electric power systems with hybrid APU," in *2016 IEEE International Power Modulator and High Voltage Conference (IPMHVC)*, 2016, pp. 434-437.

[2] H. Oyori, S. Nakagawa, H. Saito, N. Takahashi, M. Seta, and N. Morioka, "System Concept Study of Electrical Management for Onboard Systems," *SAE Technical Paper*, No. 2014-01-2200, 2014.

[3] V. P. Patel, M. Koerner, and D. Loeffelholz, "Thermal Management and Power Generation for Directed Energy Weapons," *SAE Technical Paper*, No. 2010-01-1781, 2010.

[4] S. M. Iden, M. S. Sehmbey, and D. P. Borger, "MW Class Power System Integration in Aircraft," *SAE Technical Paper*, No. 2004-01-3202, 2004.

[5] K. Shibata, T. Maedomari, K. Rinoie, N. Morioka, and H. Oyori, "Aircraft Secondary Power System Integration into Conceptual Design and Its Application to More Electric System," 2014.

[6] J. Chen, C. Wang, and J. Chen, "Investigation on the Selection of Electric Power System Architecture for Future More Electric Aircraft," *IEEE Transactions on Transportation Electrification,* vol. PP, pp. 1-1, 2018.

[7] K. Rajashekara, "Converging Technologies for Electric/Hybrid Vehicles and More Electric Aircraft Systems," *SAE Technical Paper*, No. 2010-01-1757, 2010.

[8] H. d. T. Mouton, S. M. Cox, B. McGrath, L. Risbo, and B. Putzeys, "Small-Signal Analysis of Naturally-Sampled Single-Edge PWM Control Loops," *IEEE Transactions on Power Electronics,* vol. 33, pp. 51-64, 2018.

[9] Q. Xu, P. Wang, J. Chen, C. Wen, and M. Y. Lee, "A Module-Based Approach for Stability Analysis of Complex More-Electric Aircraft Power System," *IEEE Transactions on Transportation Electrification,* vol. 3, pp. 901-919, 2017.

[10] F. Gao, X. Zheng, S. Bozhko, C. I. Hill, and G. Asher, "Modal Analysis of a PMSG-Based DC Electrical Power System in the More Electric Aircraft Using Eigenvalues Sensitivity," *IEEE Transactions on Transportation Electrification,* vol. 1, pp. 65-76, 2015.

[11] J. Kuseian. (2013, September 18, 2017). *Naval Power Systems Technology Development Roadmap* Available: http://www.navsea.navy.mil/Portals/103/Documents/Naval_Power_and_Energy_Systems_Technology_Development_Roadmap.pdf

[12] W. W. Weaver, R. D. Robinett, D. G. Wilson, and R. C. Matthews, "Metastability of Pulse Power Loads Using the Hamiltonian Surface Shaping Method," *IEEE Transactions on Energy Conversion,* vol. 32, pp. 820-828, 2017.

[13] D. G. Wilson, J. C. Neely, M. A. Cook, S. F. Glover, J. Young, and R. D. Robinett, "Hamiltonian control design for DC microgrids with stochastic sources and loads with applications," in *2014 International Symposium on Power Electronics, Electrical Drives, Automation and Motion*, 2014, pp. 1264-1271.

[14] R. D. Robinett and D. G. Wilson, "Transient stability and control of renewable generators based on Hamiltonian Surface Shaping and Power Flow Control: Part I-theory," in *2010 IEEE International Conference on Control Applications*, 2010, pp. 2196-2202.

[15] T. Deppen, B. Raczkowski, M. Amrhein, J. Wells, E. Walters, M. Bodie*, et al.*, "A Specification Analysis Framework for Aircraft Systems," *SAE International Journal of Aerospace,* vol. 9, pp. 82-90, 2016.

[16] D. Bodden, B. Eller, and S. Clements, "Integrated Electrical and Thermal Management Sub-system Optimization," *SAE Technical Paper,* No. 2010-01-1812, 2010.

[17] D. R. Forester, B. B. Malik, and S. E. Taylor, "Jet Fuel Thermal Stability - Lab Testing for JP8+100," *SAE Technical Paper,* No. 2002-01-1651, 2002.

[18] W. Lu, R. J. Mauriello, K. B. Sundaram, and L. C. Chow, "Comparison of on-resistance of a power MOSFET by varying temperature," in *Southeastcon '98. Proceedings. IEEE*, 1998, pp. 264-267.

[19] Q. Xie, D. Shin, N. Chang, and M. Pedram, "Joint Charge and Thermal Management for Batteries in Portable Systems With Hybrid Power Sources," *IEEE Transactions on Computer-Aided Design of Integrated Circuits and Systems,* vol. 35, pp. 611-622, 2016.

[20] D. Simic, "Thermal modelling, simulation and evaluation of a high power battery cell for automotive applications," in *2010 IEEE Vehicle Power and Propulsion Conference*, 2010, pp. 1-4.

[21] D. A. Corrigan and X. Liu, "Pulse Power Testing of Batteries and Supercapacitors for Hybrid Electric Vehicle Applications: A Comparison of Constant Current, Constant Power, and Ramped Power Transients," *SAE Technical Paper,* No. 2013-01-1535, 2013.

[22] M. Marracci, B. Tellini, O. Liebfried, and V. Brommer, "On the use of lithium batteries at high power pulses discharge rates," in *2016 IEEE 2nd International Forum on Research and Technologies for Society and Industry Leveraging a better tomorrow (RTSI)*, 2016, pp. 1-5.

[23] H. K. Khalil, *Nonlinear Systems* 3rd ed. Upper Saddle River, NJ 07458: Prentice Hall, 2002.

A System Model

A.1 MATLAB Initialization Script File

```
clear
clc

global R_Lm R_Ls R_po Rcp  Rcb R_m Ls Lm Lp Ub Us Up Vs
Cp Cb Cm m_Rp T0;
global R_12 K_rg C_theta1 C_theta2 alpha_m R_u T_sw Dm
Km eta_m Jm TC_O TR_O;

global h m_RLs R_Lso

global tempData loadData loadFlag



% Voltage Constants
R_Lm = 0.025; % Battery series resistance
R_Ls = 0.025; % Source series resistance
R_po = 1; %
Rcp = 1000; %
Rcb = 50;
R_m = 1000;

Ls = 0.003; % Source inductor
Lm = 0.003; % Battery inductor
Lp = 0.003; % Pulse device inductor

Ub = 0; % Battery storage device
Us = 0; % Source storage device
Up = 0; % Pulse load storage device

Vs = 270/2; % Voltage source

Cp = 0.005; % Load capacitance
Cb = 0.005; % Secondary load capacitance
Cm = 0.001; % Secondary load capacitance

m_Rp = 0.005; %
T0 = 20; % % Ambient Temperature
```

```
% Thermal Constants
R_12 = 25;
K_rg = 0.5;
C_theta1 = 1000;
C_theta2 = 100;
alpha_m = 0.05;
R_u = 10;
T_sw = 20; %

TC_O = 20;
TR_O = 20;

% Speed/Motor Constants
Dm = 0.4; %
Km = 3;
eta_m = 0.00015; %
Jm = 0.01; % Moment of inertia
h = 1;

% New Parameters
m_RLs = 0.006;
R_Lso = 0.025;


global startTime endTime power duty period delay
global    highUnstable    lowUnstable    unstableLower
unstableUpper

startTime = 0;
endTime = 60; s

% ------------------------------------------------------
---------------------
% This code performs the iterations to calculate the
unstable plots

% Range and resolution of power, duty cycle, and period
of PWM pulse power
powerSim = 500:500:10000;
dutySim = 1:1:99;
periodSim = 0.001:0.001:.25;
```

```
% 3D Stability variable declaration
unstable = zeros(length(powerSim),length(periodSim));

highUnstable = unstable;
lowUnstable = unstable;

power = powerSim(1);
period = periodSim(1);
delay = period/2;

duty = dutySim(1);

% Defining the stability boundary constraints
unstableLower = 240;
unstableUpper = 350;


% This number tracks the number of times the simulation
is ran
count = 0;
testFlag = true;
initialDuty = 0;


% Loads model into memory to increase speed
load_system('new_research_12_12_2017.slx')



% Creates an intermediate 2D stability plot to track
progress
tempPeriod = zeros(1,length(periodSim));

% Power
for j = 1:1:length(powerSim)
power = powerSim(j);

% Frequency
for i=1:1:length(periodSim)

        % Duty Cycle
            for k = 1:1:length(dutySim)
                if i == 1 && initialDuty == 0
```

```
                    sim('new_research_12_12_2017.slx')
                    clc
                    count = count + 1
                    periodSim(i)
                    powerSim(j)
                    m                                   =
unstableCheck(tout(end),endTime,i);

                    if m == 1
                        if duty > 1
                            initialDuty = duty - 1;
                            unstable(j,i) = duty - 1;

                            tempPeriod(i) = duty - 1;
                            break;
                        elseif duty == 1
                            initialDuty = duty;
                            unstable(j,i) = duty;
                            tempPeriod(i) = duty;
                            break;
                        end
                    else
                        duty = dutySim(k);
                    end
                end

                if  initialDuty  ==  0  &&  k  ==
length(dutySim)
                    initialDuty = 99;
                    unstable(j,i) = 100;
                    tempPeriod(i) = duty;
                end
            end


        if i > 1
            sim('new_research_12_12_2017.slx')
            clc
            count = count + 1
            periodSim(i)
            powerSim(j)
```

```
            m = unstableCheck(tout(end),endTime,i);

            if m == 1
                while(m == 1)
                    duty = duty - 1;
                    if duty <= 0
                        duty = 1;
                        break;
                    end
                    sim('new_research_12_12_2017.slx')
                    clc
                    count = count + 1
                    periodSim(i)
                    powerSim(j)
                    m                                   =
unstableCheck(tout(end),endTime,i);
                    if m == 0
                        break;
                    end
                end
                unstable(j,i) = duty;
                tempPeriod(i) = duty;

            elseif m == 0
                while(m == 0)
                    duty = duty + 1;
                    if duty >= 100
                        duty = 100;
                        break;
                    end
                    sim('new_research_12_12_2017.slx')
                    clc
                    count = count + 1
                    periodSim(i)
                    powerSim(j)
                    m                                   =
unstableCheck(tout(end),endTime,i);
                    if m == 1
                        break;
                    end
                end
                unstable(j,i) = duty-1;
```

```
                tempPeriod(i) = duty-1;
                duty = duty - 2;
                if duty < 1
                    duty = 1;
                end
            end

        end

    initialDuty = 0;
    period = periodSim(i);

end

period = periodSim(1);

plot(tempPeriod)

end



h = msgbox('Operation Completed');
save('unstable')
```

A.2 MATLAB Function

```
function [k] = unstableCheck(time,endtime,periodIndex)
global power  highUnstable lowUnstable

k = 0;
if time < endtime
    k = 1;
    if time < 2
        lowUnstable((power/500),periodIndex) = 1;
    else
        highUnstable((power/500),periodIndex) = 1;
    end
end

end
```

A.3 Simulink Model

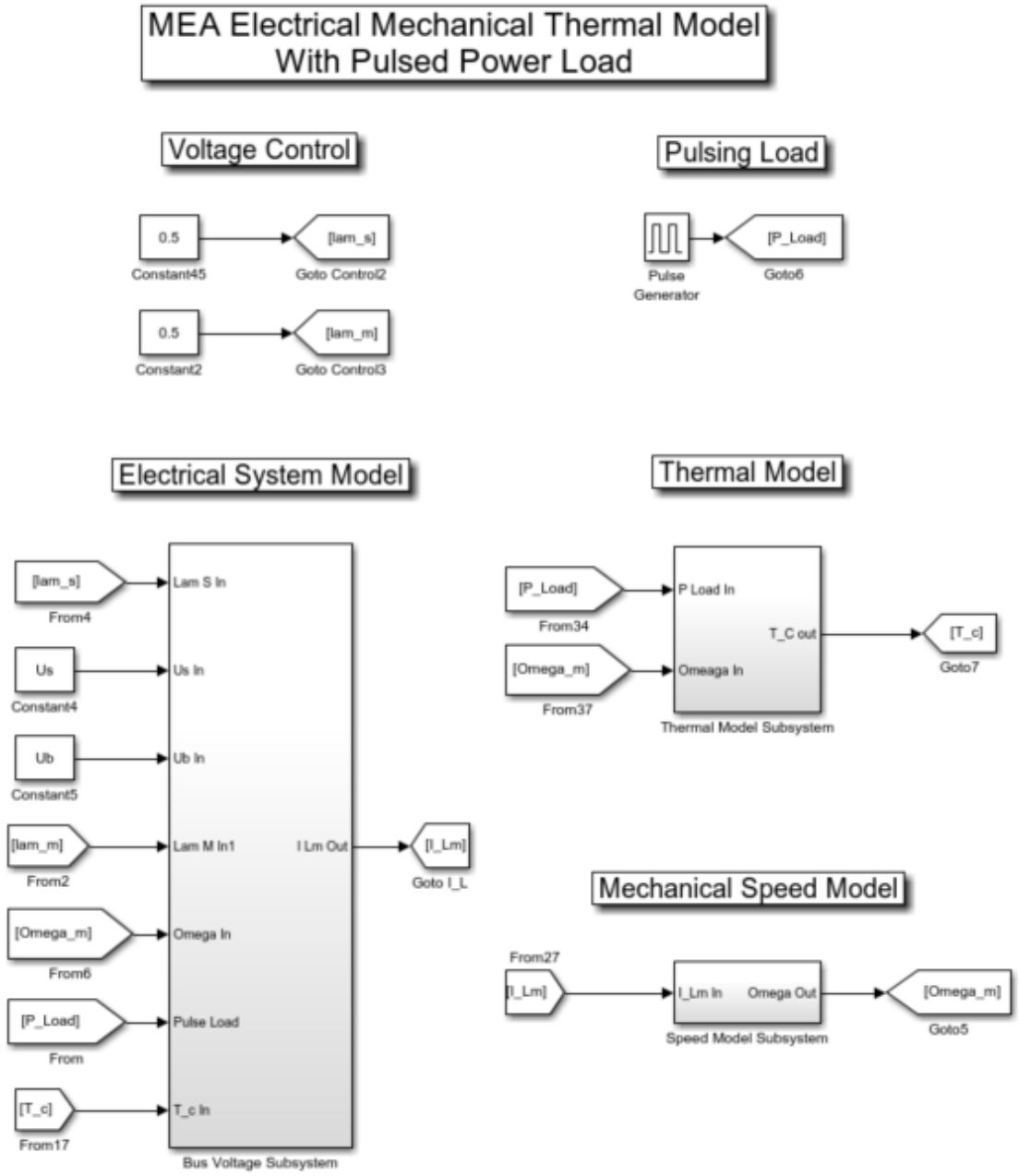

Figure A.3.1. Complete Simulink Model

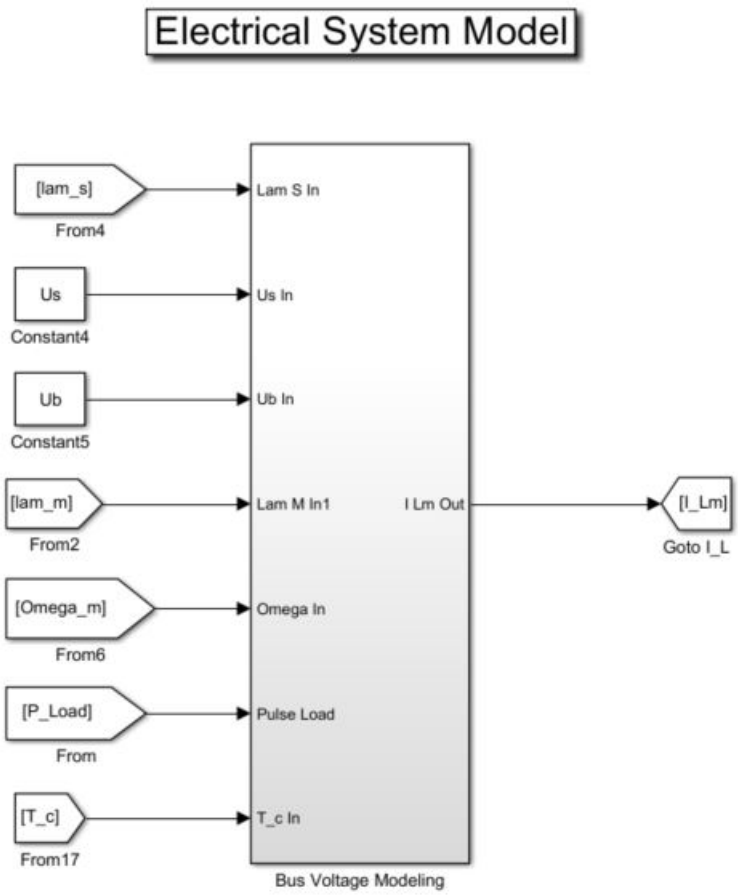

Figure A.3.2. Electrical system model subsystem with all control inputs and PMDC machine current output.

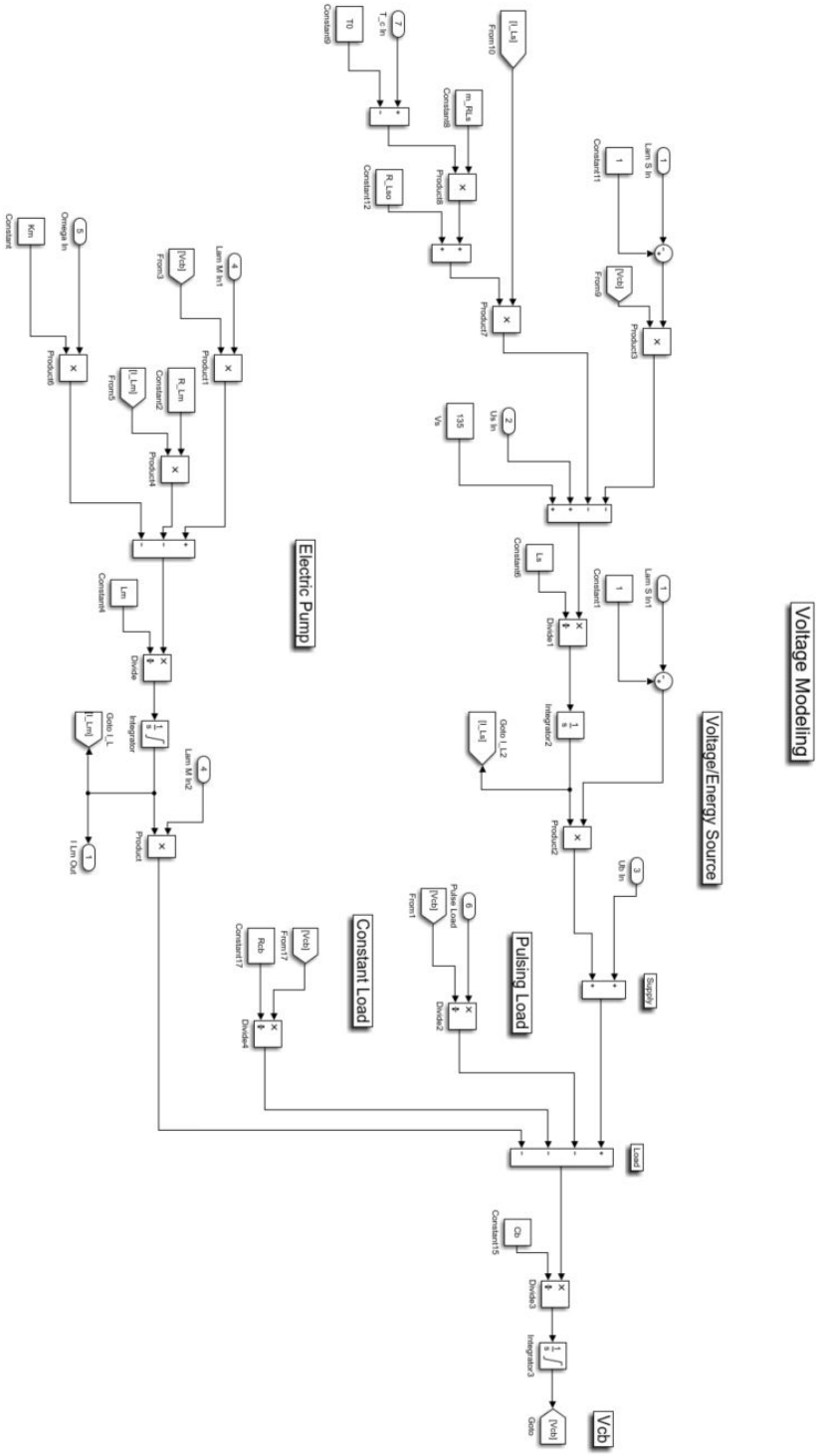

Figure A.3.3. Electrical system modeling including boost converter, constant load current, pulsing load current, and electric motor current.

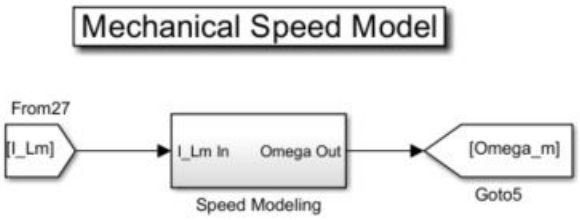

Figure A.3.4. Mechanical model subsystem.

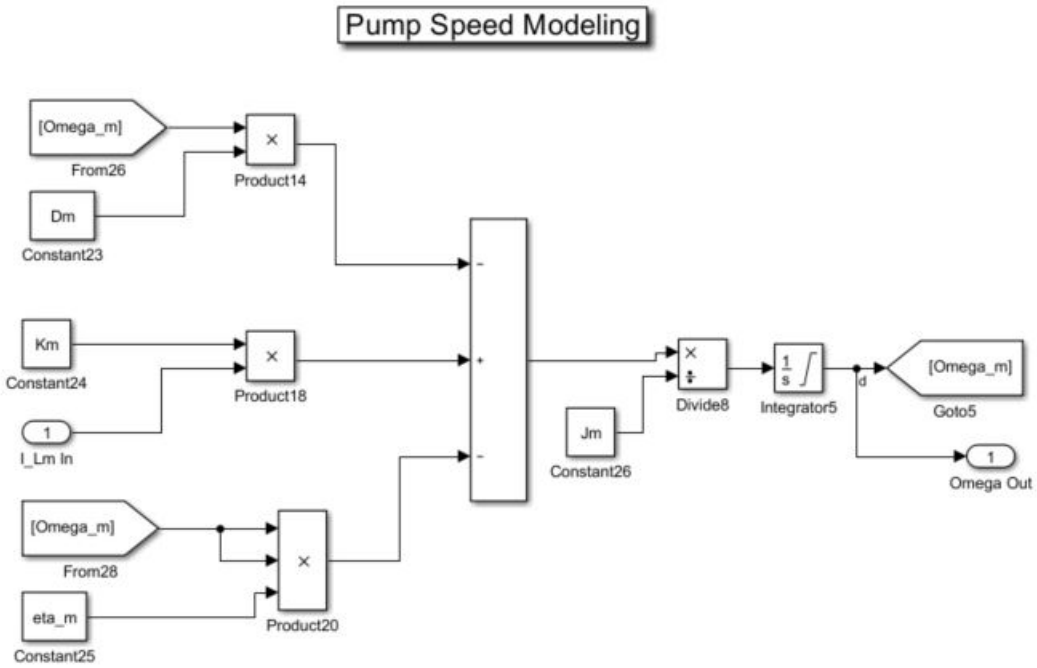

Figure A.3.5. Mechanical pump rotational speed model.

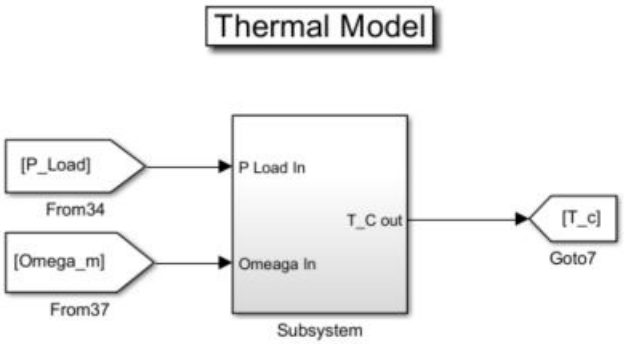

Figure A.3.6. Thermal model subsystem.

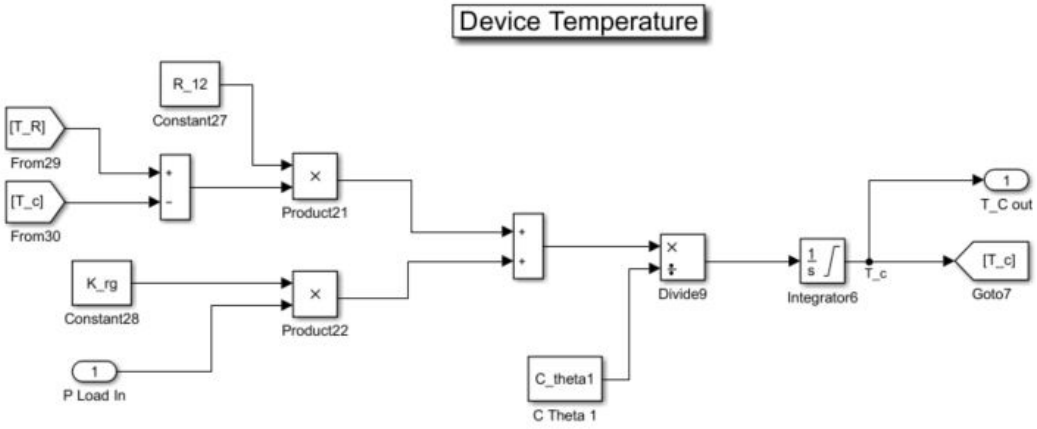

Figure A.3.7. Pulse power device temperature model.

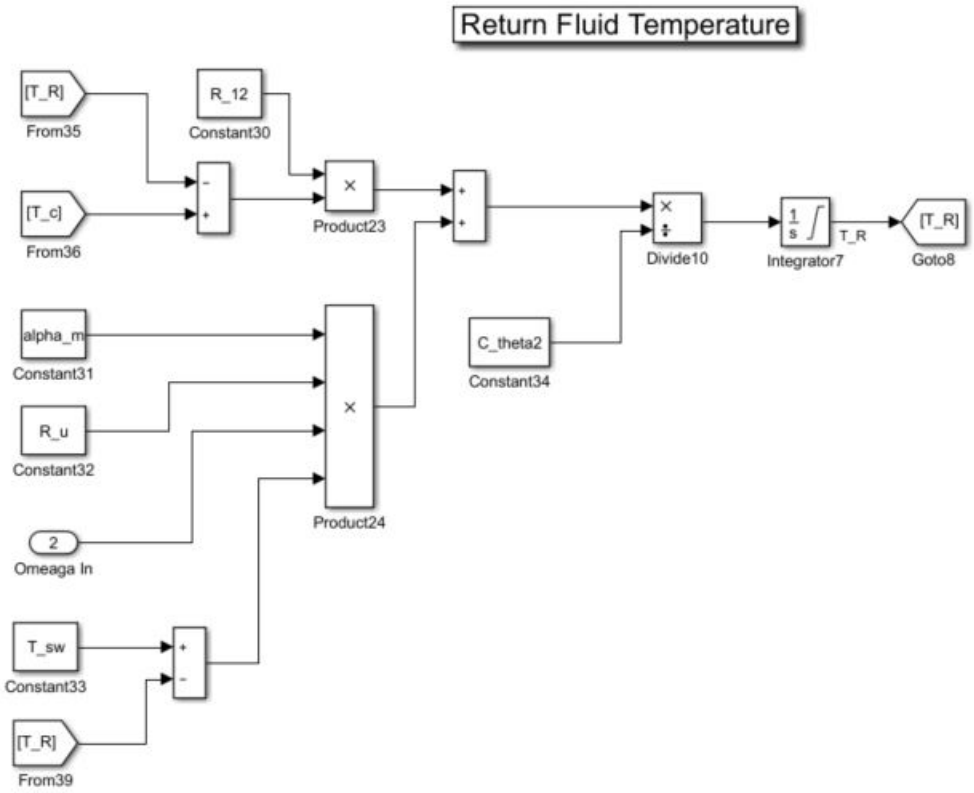

Figure A.3.8. JP8 Return fluid temperature model.

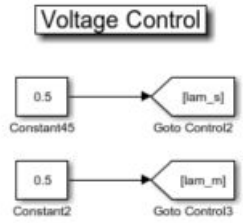

Figure A.3.9. Voltage control tags for bus boost converter and PMDC machine buck converter.

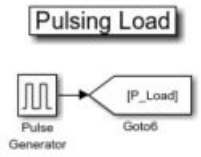

Figure A.3.10. Pulsing power load model using built in pulse generator Simulink block.

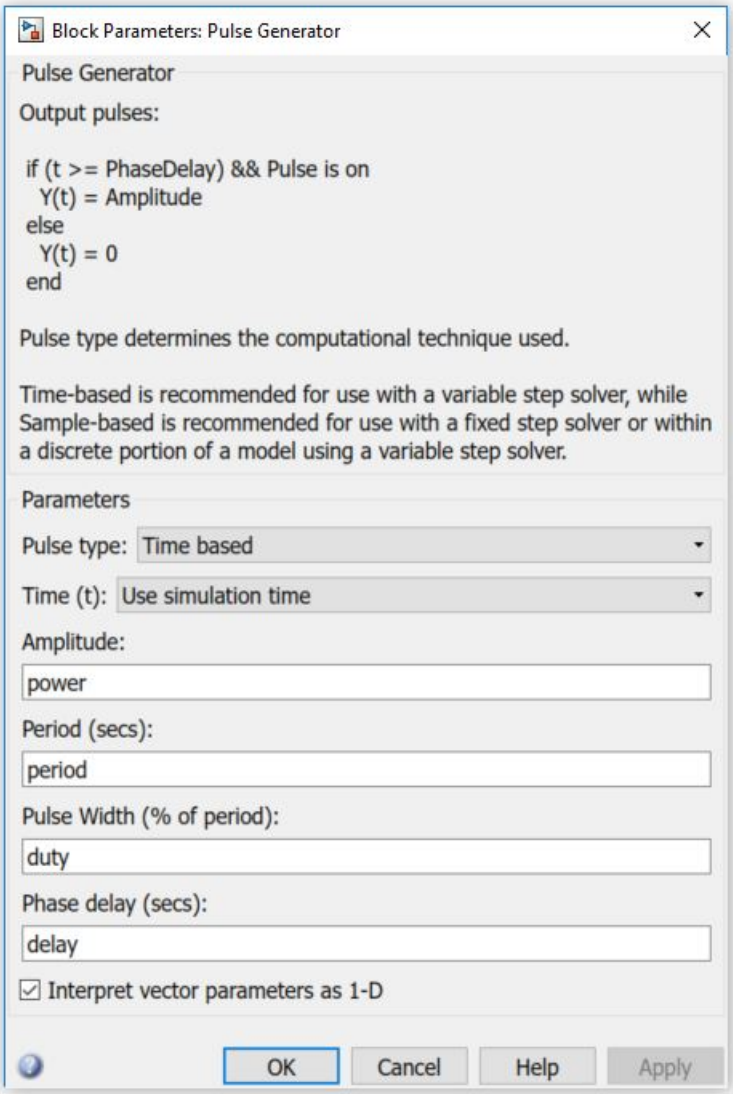

Figure A.3.11. Pulse generator parameters set as variables.

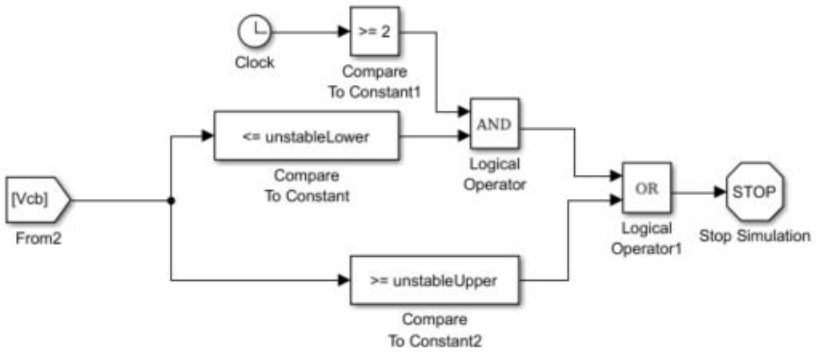

Figure A.3.12. Control model to determine when the model goes unstable given boundary conditions for the voltage.